

# Experimental Searches for the Axion and Axion-Like Particles

Peter W. Graham,<sup>1</sup> Igor G. Irastorza,<sup>2</sup>  
Steven K. Lamoreaux,<sup>3</sup> Axel Lindner,<sup>4</sup>  
and Karl A. van Bibber<sup>5</sup>

<sup>1</sup>Stanford Institute for Theoretical Physics, Stanford University, Stanford, California 94305;  
email: pwgraham@stanford.edu

<sup>2</sup>Laboratorio de Física Nuclear y Astropartículas, Departamento de Física Teórica,  
Universidad de Zaragoza, 50009 Zaragoza, Spain

<sup>3</sup>Department of Physics, Yale University, New Haven, Connecticut 06511

<sup>4</sup>DESY, 22607 Hamburg, Germany

<sup>5</sup>Department of Nuclear Engineering, University of California, Berkeley, California 94720

Annu. Rev. Nucl. Part. Sci. 2015. 65:485–514

First published online as a Review in Advance on  
August 7, 2015

The *Annual Review of Nuclear and Particle Science*  
is online at [nucl.annualreviews.org](http://nucl.annualreviews.org)

This article's doi:  
10.1146/annurev-nucl-102014-022120

Copyright © 2015 by Annual Reviews.  
All rights reserved

## Keywords

axion, axion-like particles, dark matter, microwave cavity, NMR,  
helioscope, photon regeneration

## Abstract

Four decades after its prediction, the axion remains the most compelling solution to the strong- $CP$  problem and a well-motivated dark matter candidate, inspiring a host of elegant and ultrasensitive experiments based on axion-photon mixing. This article reviews the experimental situation on several fronts. The microwave cavity experiment is making excellent progress in the search for dark matter axions in the  $\mu\text{eV}$  range and may plausibly be extended up to  $100 \mu\text{eV}$ . Within the past several years, however, researchers have realized that axions are pervasive throughout string theories, but with masses that fall naturally in the  $\text{neV}$  range, for which an NMR-based search is under development. Both searches for axions emitted from the Sun's burning core and purely laboratory experiments based on photon regeneration have recently made great progress, with ambitious projects proposed for the coming decade. Each of these campaigns has pushed the state of the art in technology, enabling large gains in sensitivity and mass reach. Furthermore, each modality has been exploited in order to search for more generalized axion-like particles, which we also discuss in this review. We are hopeful, even optimistic, that the next review of the subject will concern the discovery of the axion, its properties, and its exploitation as a probe of early universe cosmology and structure formation.

## Contents

1. INTRODUCTION .....	486
2. STRONG $CP$ AND THE AXION .....	487
3. SEARCHES FOR DARK MATTER AXIONS .....	490
3.1. Axionic Dark Matter .....	490
3.2. Cavity Microwave Experiment .....	490
3.3. ADMX and ADMX-HF .....	492
3.4. Detection with NMR: CASPER .....	497
4. SEARCHES FOR SOLAR AXIONS .....	500
4.1. Solar Axions .....	500
4.2. Axion Helioscopes .....	502
4.3. CAST .....	502
4.4. IAXO .....	504
5. PURELY LABORATORY EXPERIMENTS .....	505
5.1. Light-Shining-Through-Walls Experiments with Microwaves, Optical Photons, and X-Rays .....	506
5.2. The Future of Light-Shining-Through-Walls Experiments .....	507
6. SUMMARY AND CONCLUSIONS .....	509

## 1. INTRODUCTION

Since the axion was predicted in 1978 (1, 2), there has been a steady crescendo of interest in this particle, and a coordinated global effort to find it is finally taking shape. Should the axion ultimately be discovered, it would finally resolve one of the last outstanding questions in the Standard Model of particle physics; specifically, it would validate the Peccei–Quinn (PQ) mechanism to protect the strong interaction from  $CP$ -violating effects (3, 4), as evidenced by the absence of a neutron electric dipole moment (EDM). Furthermore, the axion may be discovered as the dark matter halo of our Galaxy, the Milky Way, thereby answering the question of what constitutes the predominant form of matter in our Universe. This article is an experimental review, focusing on new concepts and developments since the last such reports in this journal (5) and in others (6, 7). The reader is referred to several excellent theory reviews (8–12) that are still largely up to date. There is one new development of interest to our present purpose, however, namely the realization that any string theory contains several and perhaps a large number of axion-like particles (ALPs), although they are extremely light—of order  $\text{neV}$ . We briefly discuss this topic in Section 3.4, before describing the NMR-based experiment to search within that mass region. Nevertheless, some theoretical preliminaries are in order; therefore, we begin this review in Section 2 by describing the basic physics underlying the axion and its phenomenology. At the beginning of Section 3, we introduce constraints on the axion’s mass and couplings, primarily from its cosmological production and astrophysics, in preparation for our discussion of the microwave cavity experiment. In Section 4 we discuss axion–photon mixing within a magnetic field in the relativistic limit relevant to both solar searches and laboratory experiments, along with axion emission from the Sun’s burning core.

Whereas this review concerns primarily the axion solving the strong- $CP$  problem, it also deals with more generalized ALPs accessible to these experiments. As we are writing from the experimental perspective, after all, one should be open to surprises!

## 2. STRONG CP AND THE AXION

The gauge sector of the Standard Model of electroweak interactions is among the most successful theories in the history of physics, whereas the flavor sector is still incomplete, with known issues and uncertainties, such as the neutrino mass spectrum. Perhaps the most mysterious issue is that of the so-called strong- $CP$  problem [combined charge conjugation ( $C$ ) and parity inversion ( $P$ ) symmetry or, equivalently, time-reversal ( $T$ ) symmetry]: Why does the quantum chromodynamic (QCD) Lagrangian conserve  $CP$  symmetry (or, equivalently,  $T$  symmetry) apparently perfectly, to within extraordinarily strict experimental limits, when there is no fundamental reason to exclude possible symmetry-nonconserving interactions?

As described in Reference 13, this problem can be understood as follows: The Lagrangian of the electromagnetic field

$$-\frac{1}{4}F_{\mu\nu}F_{\mu\nu} = \frac{1}{2}(\vec{E}^2 - \vec{B}^2) \quad 1.$$

can comprise other Lorentz scalars, such as (14)

$$F_{\mu\nu}\tilde{F}_{\mu\nu}, \quad \tilde{F}_{\mu\nu} = \frac{1}{2}\epsilon_{\mu\nu\kappa\lambda}F_{\kappa\lambda}. \quad 2.$$

This scalar violates both  $P$  and  $T$  invariance, as evident from its three-dimensional form:

$$F_{\mu\nu}\tilde{F}_{\mu\nu} = -4\vec{E} \cdot \vec{B}. \quad 3.$$

However, this scalar generates no observable effects in electrodynamics because it is a four-divergence and the fields fall off rapidly toward infinity.

The corresponding possible  $P$ - and  $T$ -violating term in the QCD Lagrangian, known as the  $\theta$  term, is usually written as

$$L_\theta = -\theta(\alpha_s/8\pi)\tilde{G}_{\mu\nu}^a G_{\mu\nu}^a, \quad 4.$$

where  $\alpha_s \sim 1$  is the coupling constant for the gluon field  $G$  and is the QCD analog of the fine-structure constant  $\alpha = 1/137$  in electrodynamics. Whereas the four-divergence of this term can remain zero, implying that dynamics are not directly affected by it, both the chiral anomaly and the self-interaction of the gluon vector potential field configurations, which do not fall off rapidly enough at infinity, can lead to observable effects.

Most famously, the  $\theta$  term provides a contribution to the neutron EDM, which is estimated in References 15 and 16. First, a chiral rotation  $\psi \rightarrow \exp(-i\gamma_5\theta)\psi$  of the quark spinor fields  $\psi$  transforms the  $\theta$  term away. Under this rotation, the mass term in the Hamiltonian of the light quarks,  $u$ ,  $d$ , and  $s$ ,

$$m_u\bar{u}u + m_d\bar{d}d + m_s\bar{s}s \quad 5.$$

acquires a  $CP$ -odd term,

$$\delta H_{CP} = i\theta \frac{m_u m_d m_s}{m_u m_d + m_u m_s + m_d m_s} (\bar{u}\gamma_5 u + \bar{d}\gamma_5 d + \bar{s}\gamma_5 s). \quad 6.$$

Because the  $s$  quark is much heavier than the  $u$  and  $d$  quarks, the mass factor simplifies to

$$\frac{m_u m_d m_s}{m_u m_d + m_u m_s + m_d m_s} \approx \frac{m_u m_d}{m_u + m_d}. \quad 7.$$

The  $CP$ -odd  $\pi NN$  vertex generated by this Hamiltonian can be transformed by use of the partially conserved axial-current (PCAC) technique to

$$\langle \pi^a N_f | \delta H_{CP} | N_i \rangle = -\theta \frac{m_u m_d}{m_u + m_d} \frac{\sqrt{2}}{f_\pi} \langle N_f | \bar{q} \tau^a q | N_i \rangle, \quad 8.$$

where  $\tau^a$  is the isotopic spin operator and  $f_\pi = 130$  MeV is the pion decay constant. The nucleon matrix element  $\langle p | \bar{u}d | n \rangle$  is related through SU(3) symmetry to the mass splitting in the baryon octet:

$$\langle p | \bar{u}d | n \rangle = \bar{p}n \frac{M_\Xi - M_\Sigma}{m_s} \approx \bar{p}n, \quad 9.$$

where  $p$  and  $n$  are the Dirac spinors of the proton and neutron, respectively, and  $M_\Xi$  and  $M_\Sigma$  are the masses of the  $\Xi$  and  $\Sigma$  hyperons, respectively. The full  $\pi NN$  interaction can be now be described by an effective Hamiltonian:

$$H_{\pi NN} = \bar{\pi} \tilde{N} \vec{\tau}(i \gamma_5 g_{\pi NN} + \bar{g}_{\pi NN}) N, \quad 10.$$

where the  $CP$ -odd constant is

$$\bar{g}_{\pi NN} = -\theta \frac{m_u m_d}{m_u + m_d} \frac{\sqrt{2}}{f_\pi} \frac{M_\Xi - M_\Sigma}{m_s} \approx -0.027\theta. \quad 11.$$

The  $CP$ -even  $\pi NN$  constant in the effective Hamiltonian is known:

$$g_{\pi NN} = 13.6. \quad 12.$$

A crucial observation (16) is that in the chiral limit  $m_\pi \rightarrow 0$  the neutron EDM can be expressed exactly via  $\bar{g}_{\pi NN}$  and  $g_{\pi NN}$ . In this limit, there are only two diagrams that are singular in the pion mass and thus contribute to the EDM. In these diagrams, a  $\pi NN$  vertex is the strong pseudoscalar coupling, with the coupling constant  $g_{\pi NN} \sqrt{2}$ , and the second is a  $CP$ -odd scalar, with the coupling constant  $\bar{g}_{\pi NN} \sqrt{2}$ . The contribution of these diagrams to the neutron EDM is

$$d_n = \frac{|e|}{m_p} \frac{g_{\pi NN} \bar{g}_{\pi NN}}{4\pi^2} \ln \frac{m_\rho}{m_\pi} = -3.3 \times 10^{-16} \theta \text{ (e cm)}. \quad 13.$$

The choice of the  $\rho$  meson mass,  $m_\rho = 770$  MeV, as the typical hadronic scale at which the logarithmic integral is cut off is somewhat arbitrary. The chiral parameter, the logarithm in Equation 13, is not large for any reasonable cutoff and is only 1.7 when  $m_\rho$  is used. Due to the absence of other terms that are logarithmic in  $m_\pi$ , a coincidental mutual cancellation between this contribution and possible others appears unlikely. Therefore, Equation 13 can be considered a conservative estimate of the neutron EDM.

Combining this estimate with the most sensitive experimental result given in Reference 17,  $d_n < 2.9 \times 10^{-26}$  e cm, sets a very strict upper limit for the  $CP$ -odd QCD parameter:

$$|\theta| < 9 \times 10^{-11}. \quad 14.$$

This is the strong- $CP$  problem: There is no natural explanation for the extreme smallness of the parameter  $\theta$ , and this is considered to be a fine-tuning problem. Indeed, it appears particularly unnatural when one considers that  $\theta$  is renormalized by other  $CP$ -odd interactions (e.g., known  $CP$  violation in  $K$  meson decay), and in general its renormalization can be infinite. In the Standard Model, the induced contributions to  $\theta$  almost certainly diverge logarithmically starting at fourteenth (!) order in the electroweak coupling constant (18, 19). Therefore, as a technicality,  $\theta$  cannot be calculated.

One solution to this problem, which is quite obvious from Equation 6, is to assume that one of the quark masses is zero or very small (lighter than a neutrino). This assumption apparently contradicts experimental data, although that is not entirely certain.

A solution to the strong- $CP$  problem that has attracted wide interest, particularly in the context of this review, is to leave the  $\theta$  term as it is but to somehow make it irrelevant. One can do so by introducing an extra global symmetry into the theory (3, 4), that is, by considering  $\theta$  as a field, not a fixed parameter. Such a symmetry leads in turn to the prediction of a new light pseudoscalar

particle, the axion (1, 2). In a restricted sense, the axion plays a role similar to that of the Higgs boson; the  $CP$ -violating interaction cannot be calculated in the context of the Standard Model and in fact diverges without the axion, whereas electroweak interactions beyond first order diverge without the (now discovered!) Higgs boson. Of course, it would be incorrect to say that the axion is as well motivated as the Higgs boson; however, the parallelism should be noted. The mass of the axion is unknown, but is bound from both above and from below by experiments and observations.

Essentially all of the physics of the axion depends on a large unknown energy scale  $f_a$ , at which PQ symmetry is broken; in the low-energy limit of this theory, the nonperturbative vacuum structure of QCD drives the parameter of the  $CP$ -violating term to the  $CP$ -conserving minimum, with the axion resulting from the remnant oscillations of the axion field about this minimum. The mass of the axion is given by (9–11)

$$m_a \approx 6 \text{ eV} \left( \frac{10^6 \text{ GeV}}{f_a} \right). \quad 15.$$

In its original form, the PQ symmetry-breaking scale was posited (for no compelling reason) to be of order the electroweak scale,  $f_{EW}$ , implying very heavy axions ( $\sim 100$  keV), which were quickly ruled out by accelerator- and reactor-based experiments. More general models were then constructed of much higher values of  $f_a$  and much smaller  $m_a$ .

Generically, all the couplings of the axion to radiation and matter are also inversely proportional to  $f_a$ . The axion–photon coupling is of special interest here, as virtually all of the most sensitive search strategies are based on the coherent mixing of axions and photons in a strong magnetic field. Being a pseudoscalar ( $J^\pi = 0^-$ ), the axion has a two-photon coupling whose strength is given by

$$g_{a\gamma\gamma} = \frac{\alpha g_\gamma}{\pi f_a}, \quad 16.$$

where  $g_\gamma$  is a dimensionless model-dependent parameter of order unity,  $g_\gamma = -0.97$  in the Kim–Shifman–Vainshtein–Zakharov (KSVZ) model (20, 21), and  $g_\gamma = 0.36$  in the Dine–Fisher–Srednicki–Zhitnisky (DFSZ) model (22, 23). These values are representative within broad classes of hadronic and Grand Unification Theory (GUT)-inspired axions, underlining an important feature of the theory that the dimensionless axion–photon coupling  $g_\gamma$  is highly insensitive to the specific axion model. This observation extends even to axions intrinsic to the string theory structure (24).<sup>1</sup>

As explained above, there is a strong physics case for the axion, but it may be simply the first known representative of a new particle family of so-called weakly interacting slim particles (WISPs). Such WISPs are motivated, for example, by string-theory-inspired extensions of the Standard Model, which predict, among other things, the existence of ALPs and hidden photons (HPs) (25). Although they are entirely unrelated to the strong- $CP$  problem, ALPs and HPs may also be viable dark matter candidates (26, 27). ALPs are of special interest because there are a number of different astrophysics phenomena, such as the transparency of the Universe to TeV photons (28, 29) and the evolution of stars (30, 31), that might point to the existence of very light ALPs with a coupling strength detectable by the next generation of helioscopes and purely laboratory experiments. Note that the ongoing discussion on the validity of naturalness (questioning arguments for the existence of new particles on the basis of fine-tuning issues) triggered by the results of the first run of the Large Hadron Collider (LHC) (see, e.g., References 32 and 33)

<sup>1</sup>Reference 24 erroneously implies that  $g_\gamma^{\text{STRING}} = (1/4)g_\gamma^{\text{DFSZ}}$ ; however, the author later clarified that  $g_\gamma$  within string models should be exactly equal to that of the most generic model, DFSZ, and that it represents a strict lower limit to the coupling [E. Witten, personal communication (2007)].

does not influence the hints for WISPs as sketched here. Thus, the parameter space for very light and very feebly interacting particles is opening up next to the axion region, and experiments are encouraged to widen their field of view accordingly.

### 3. SEARCHES FOR DARK MATTER AXIONS

#### 3.1. Axionic Dark Matter

A sufficiently light axion represents an excellent dark matter candidate (34), as its density relative to the critical density of the Universe is given by

$$\Omega_a \approx \left( \frac{6 \mu\text{eV}}{m_a} \right)^{\frac{7}{6}}. \quad 17.$$

An axion of  $m_a \approx 20 \mu\text{eV}$  (within a factor of approximately two) would thus account for the entire dark matter density of the Universe,  $\Omega_m \approx 0.27$ . Without tuning of the initial misalignment angle, much lighter axions would overclose the Universe; therefore,  $m_a \approx 1 \mu\text{eV}$  may be considered a strong lower limit on the axion mass  $m_a$ . There has been a lingering controversy about the relative contribution between axion production from the vacuum realignment mechanism and radiation from topological defects (axion strings, domain walls). A definitive resolution in the near future is unlikely, but the current general consensus is that the sum of all contributions to  $\Omega_a$  could increase the axion mass corresponding to  $\Omega_{\text{DM}}$  by two orders of magnitude. As we are presently interested only in establishing conservative ranges for experiments, searches should plan on reaching the  $\mu\text{eV}$  scale. Cosmology also provides an upper bound on the axion mass by the production of thermal axions, the hot dark matter limit of approximately 1 eV, but this topic does not concern us here.

Stellar evolution also places strict limits on axions (35). Axions of mass exceeding  $\sim 16 \text{ meV}$  would have quenched the neutrino pulse observed from SN1987a, thus bounding the axion mass from above. The best indirect stellar bound on the axion–photon coupling comes from galactic globular clusters,  $g_{a\gamma\gamma} < 0.66 \times 10^{-10} \text{ GeV}^{-1}$ . This bound recently surpassed the best direct stellar bound, from the CERN Axion Solar Telescope (CAST) search for solar axions,  $g_{a\gamma\gamma} \approx 0.88 \times 10^{-10} \text{ GeV}^{-1}$  (discussed in Section 4). For PQ axions, such couplings correspond to masses far in excess of the open mass region (i.e.,  $10^{-6} \text{ eV} < m_a < 10^{-2} \text{ eV}$ ) and, thus, are not germane to the dark matter problem. In recent years, a modest literature has suggested that the luminosity function of white dwarfs (degenerate stars undergoing gravothermal cooling) may require an additional cooling mechanism that could be accounted for by axions in the  $\sim 10\text{-meV}$  range (36–38). The evidence is far from compelling; moreover, such masses are beginning to encroach on the region disfavored by SN1987a.

The range  $10^{-6}\text{--}10^{-2} \text{ eV}$  has traditionally been considered the open mass window for axions (Figure 1) (39). However, as mentioned above, string theories are replete with axions or ALPs—more than 100 within any particular realization—but such theories naturally favor  $f_a \approx 10^{15}\text{--}10^{16} \text{ GeV}$ , corresponding to neV-scale masses. It is impossible to say which, if any of these, solves the strong- $CP$  problem and which, if any, would be cosmologically significant. We briefly review string theory axions and possible limits from isocurvature fluctuations in Section 3.4 as a preamble to our discussion of the NMR-based CASPEr (Cosmic Axion Spin Precession Experiment).

#### 3.2. Cavity Microwave Experiment

Problematically, such light axions would be so weakly coupled as to be undetectable in conventional experiments. In the 1980s, Sikivie (40, 41) resolved this conundrum by showing that axions

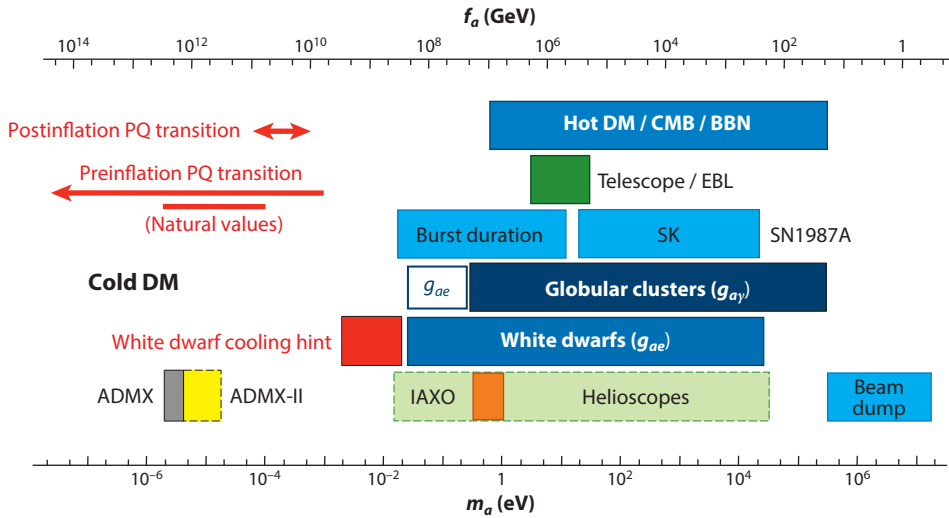


**Figure 1**

Limits on the axion mass established by cosmology and astrophysics. The limits on cold dark matter (cold DM) indicated by the red lines are particularly uncertain. Abbreviations: BBN, Big Bang nucleosynthesis; CMB, cosmic microwave background; DM, dark matter; EBL, extragalactic background light; PQ, Peccei–Quinn; SK, Super-Kamiokande. Modified with permission from Reference 39. Copyright 2014, Particle Data Group.

constituting the Milky Way halo could resonantly convert into a monochromatic microwave signal in a high-quality-factor ( $Q$ ) microwave cavity permeated by a strong magnetic field, with the conversion power given by

$$P_{\text{SIG}} = \eta g_{a\gamma\gamma}^2 \left( \frac{\rho_a}{m_a} \right) B_0^2 V C Q_L. \quad 18.$$

The physics parameters, beyond the control of the experimentalist, are the axion–photon coupling constant  $g_{a\gamma\gamma}$ , the axion mass  $m_a$ , and the local density of axions in the halo  $\rho_a$ . Within experimental control are the magnetic field strength  $B_0$  and the volume of the cavity  $V$ , as well as the mode-dependent form factor  $C$  and the loaded quality factor of the cavity  $Q_L$ —that is, the quality factor with power coupled out to the receiver.  $\eta$  is the fraction of power coupled out by the antenna probe, generally adjusted to be at or near critical coupling:  $\eta = 1/2$ . The resonant conversion condition is that the frequency of the cavity must equal the mass of the axion:  $h\nu = m_a c^2 [1 + \frac{1}{2} \mathcal{O}(\beta^2)]$ , where  $\beta \approx 10^{-3}$  is the galactic virial velocity. The signal is thus monochromatic to  $10^{-6}$ . The search is performed by tuning the cavity in small overlapping steps (**Figure 2**).

The expected signal power is extraordinarily tiny, of order  $10^{-22}$  W for the current experiment. Actual detection of the axion is the consummate signal-processing problem, governed by the Dicke radiometer equation (42),

$$\frac{S}{N} = \frac{P_{\text{SIG}}}{k T_{\text{SYS}}} \sqrt{\frac{t}{\Delta\nu}}, \quad 19.$$

where  $S/N$  is the signal-to-noise ratio and the total system noise temperature,  $T_{\text{SYS}} = T + T_N$ , is the sum of the physical temperature  $T$  and the intrinsic amplifier noise temperature  $T_N$ , with  $k$  the Boltzmann constant. The integration time is  $t$ , and the bandwidth of the axion signal is  $\Delta\nu$ , assuming that the resolution of the spectral receiver is much better than the width of the axion signal.

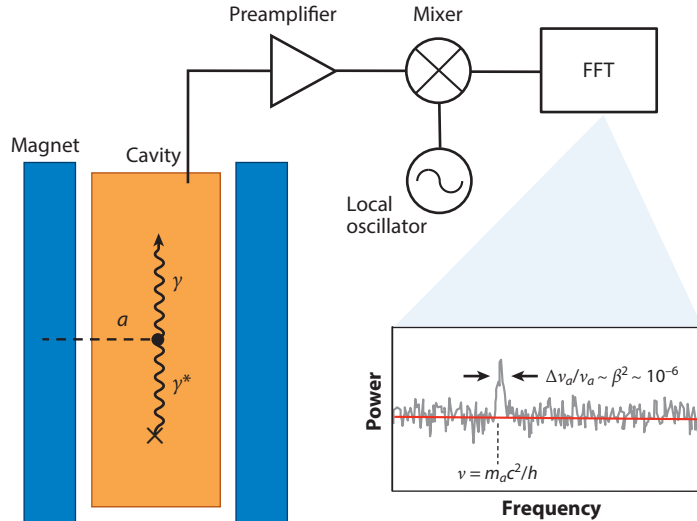


**Figure 2**

Schematic of the microwave cavity search for dark matter axions. Axions resonantly convert to a quasi-monochromatic microwave signal in a high- $Q$  cavity in a strong magnetic field; the signal is extracted from the cavity by an antenna, amplified, and mixed down to the audio range, and the power spectrum is then calculated by a fast Fourier transform (FFT). Possible fine structure on top of the thermalized axion spectrum would reveal important information about the formation of our Galaxy. Modified from Reference 54 with permission.

An especially important characteristic of the microwave cavity search for axions that strongly differentiates it from searches for weakly interacting massive particles (WIMPs) is that it is a total energy detector; that is, the signal represents the instantaneous (mass plus kinetic) energy of the axion. Whereas the majority of the signal strength will almost certainly be found in a broad quasi-Maxwellian distribution of width  $\Delta\nu/\nu \sim 10^{-6}$ , there has been a great deal of speculation and research over the past two decades about the phase-space structure of the axion signal, caustics, fine structure due to late infall axions, and so on (43). A high-resolution channel has been implemented in the Axion Dark Matter eXperiment (ADMX) based on a fast Fourier transform (FFT) of an entire subspectrum, the basic unit of data collection, which can resolve structure down to the transform limit, for example,  $\Delta\nu/\nu \sim 10^{-11}$  for a 100-s run at 1 GHz. Due to the motion of the laboratory through the dark matter halo ( $v_{\text{ROT}} \sim 0.4 \text{ km s}^{-1}$ ,  $v_{\text{ORB}} \sim 30 \text{ km s}^{-1}$ ), any fine structure would exhibit both diurnal and sidereal modulations in frequency. A little reflection makes it clear that, should such fine structure be found, fitting the amplitude and phase of the diurnal and sidereal oscillation in frequency would uniquely determine each vector flow to high precision, truly opening up the field of dark matter astronomy (44). Whereas  $N$ -body simulations strongly support a hierarchical and chaotic picture of structure formation, these simulations themselves exhibit significant mesoscale substructure in phase space, which could be studied.

### 3.3. ADMX and ADMX-HF

In this section, we describe the evolution of the microwave cavity experiment and its supporting technologies, from the early pilot experiments in the late 1980s to the present day.

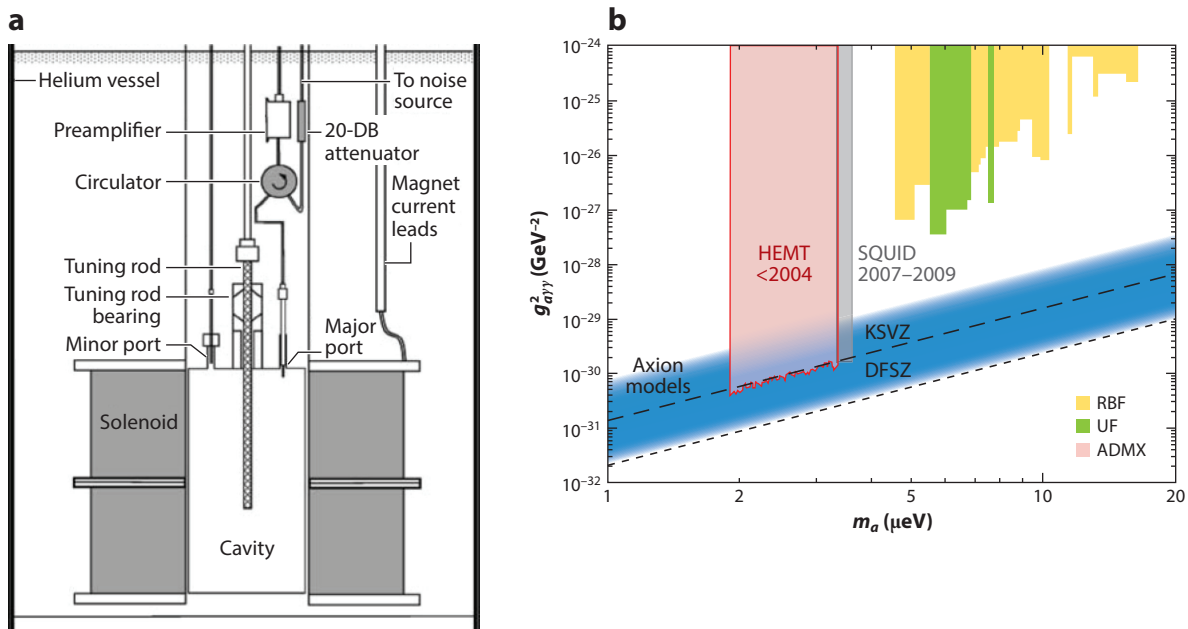


**Figure 3**

(a) Layout of the RBF experiment. (b) The 90%-CL exclusion regions for ADMX and the RBF and UF experiments. Abbreviations: HEMT, high-electron-mobility transistor; SQUID, superconducting quantum interference device. Panel *a* modified with permission from Reference 45. Copyright 1989, American Physical Society. Panel *b* modified with permission from Reference 46. Copyright 1990, American Physical Society.

**3.3.1. Early experiments.** Two pilot efforts in the 1–4-GHz range, at Brookhaven National Laboratory (BNL) (45, 46) and the University of Florida (UF) (47), were mounted soon after publication of the experimental concept. These employed cavities with a volume of a few liters, as well as the best conventional amplifiers at that time, such as heterojunction field effect transistor (HFET) amplifiers. With noise temperatures in only the  $\sim 3$ –20-K range, these amplifiers were not sensitive enough to reach PQ axions (**Figure 3**). Nevertheless, these two experiments developed much of the design philosophy and knowhow about microwave cavities that the current experiments still build on today.

The CARRACK experiment in Kyoto, Japan, marked another significant development in the history of the microwave cavity experiment. The goal of CARRACK was to significantly decrease the system noise temperature, both by reducing the physical temperature of the experiment down to  $\sim 15$  mK with a  $^3\text{He}$ - $^4\text{He}$  dilution refrigerator and by utilizing a Rydberg-atom single-quantum detector in lieu of a standard linear amplifier to eliminate the amplifier noise contribution. Linear amplifiers are ultimately subject to an irreducible noise contribution, the standard quantum limit (SQL):  $kT_{\text{SQL}} = h\nu$ . The Rydberg-atom single-quantum detector can effectively be considered a tunable radio-frequency (RF) photomultiplier tube, for which the photon interacts as a particle rather than a wave, thereby circumventing the SQL. Tada et al. (48) measured the blackbody photon spectrum of the cavity at 2.527 GHz as a function of temperature all the way down to  $T = 67$  mK, nearly a factor of two below the SQL of  $\sim 120$  mK. From the technical perspective, CARRACK was successful, but it ultimately proved too complex to be feasible as a production experiment.

**3.3.2. ADMX.** Drawing on the experience of the Rochester–BNL–Fermilab (RBF) and UF searches, the ADMX Collaboration designed an experiment with the goal to reach KSVZ axions saturating our galactic halo, whose local density would be  $\rho_a \sim 0.45 \text{ GeV cm}^{-3}$ . This goal would be achieved both by scaling up the cavity volume by two orders of magnitude and by profiting from the steady improvement in the noise temperature of commercial HFET amplifiers.

The NbTi superconducting magnet has an inner bore with dimensions  $60 \text{ cm} \times 110 \text{ cm}$ , and it sustains a maximum central field of 8 T. The microwave cavities are made by electrodepositing high-purity copper on a stainless steel body, followed by annealing (**Figure 4**), leading to cavity

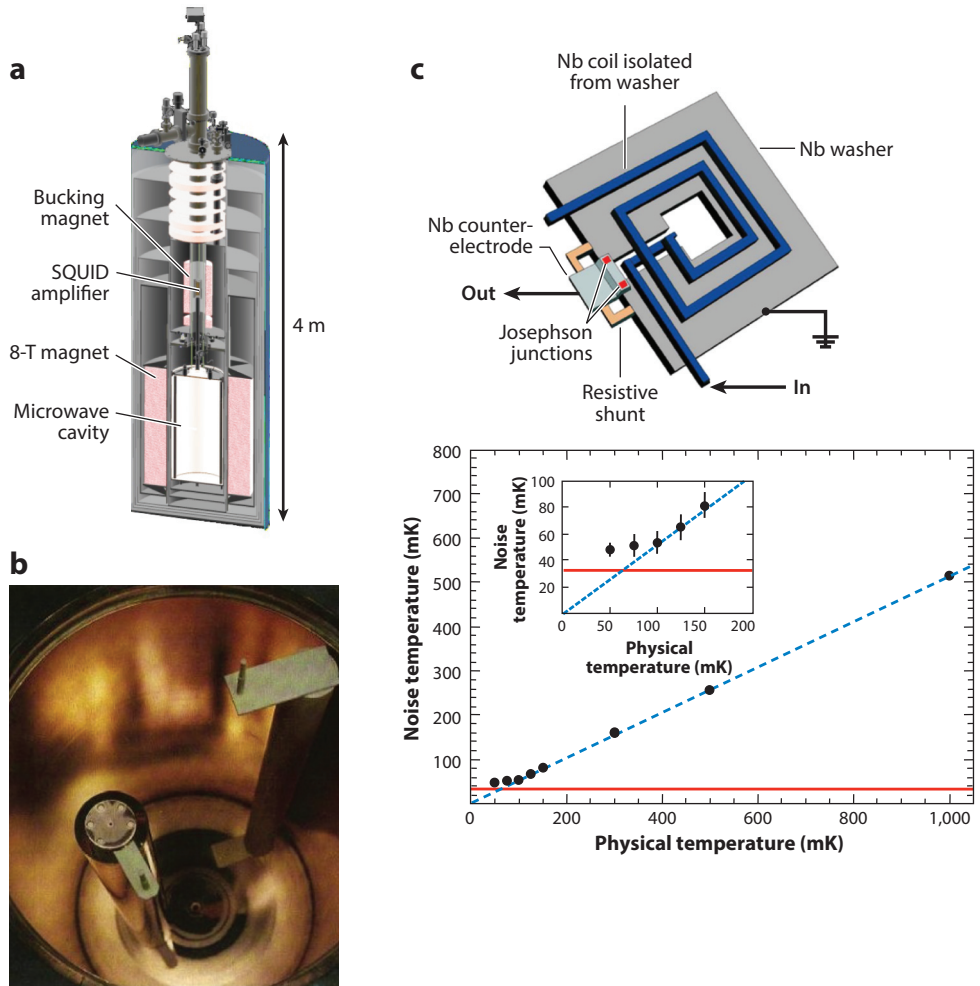


**Figure 4**

ADMX. (a) Schematic layout. (b) Microwave cavity and tuning rods. (c) dc superconducting quantum interference device (SQUID) amplifiers. In addition to being near-quantum limited, the microstrip-coupled SQUID amplifiers have been demonstrated to be tunable, can work with a reactive load, and can be staged (49–51). Top image in panel *c* modified with permission from Reference 51. Copyright 2000, American Physical Society. Bottom image in panel *c* modified with permission from Reference 52. Copyright 2011, American Physical Society.

quality factors of  $\sim 10^5$ ; the experiment is tuned in small overlapping steps of the cavity bandpass. To date, the experiment has been cooled to superfluid helium temperatures of  $\sim 1.5$  K.

For the first operational phase of ADMX (1995–2004), HFET amplifiers made by the National Radio Astronomical Laboratory (NRAO) were used, ultimately reaching a noise temperature ( $T_N$ ) of  $\sim 1.5$  K; the system noise temperature ( $T_{\text{SYS}}$ ) was thus  $\sim 3$  K. For the second operational phase (2007–2009), microstrip-coupled superconducting quantum interference device (SQUID) amplifiers (MSAs) developed specifically for ADMX were employed; their noise temperature was demonstrated on the bench to be  $< 1.5 T_{\text{SQL}}$  at frequencies up to 1 GHz, when cooled to 30 mK (49–51). However, the noise of these MSAs exhibits a strong temperature dependence, and at pumped helium temperatures they perform no better than transistor-based amplifiers (**Figure 4**). Nevertheless, demonstrating that dc SQUID amplifiers could be made to work successfully in situ represented a great advance for the experiment. A dilution refrigerator will be incorporated into the experiment in 2015, enabling ADMX to achieve  $T_{\text{SYS}} < 200$  mK, a temperature sufficiently low to enable detection of DFSZ axions even with less than saturation density.

To date, ADMX has covered 460–890 MHz in frequency (1.9–3.65  $\mu\text{eV}$ ), or slightly less than an octave in mass range (**Figure 3**) (53, 54). This range underscores the importance of (a) concurrent research and development (R&D) on new cavity and amplifier concepts for frequencies much greater than 1 GHz and (b) the need to greatly increase the scanning rate of the experiment.

**3.3.3. ADMX-HF.** A second, smaller ADMX platform has been constructed and commissioned at Yale University, precisely to develop technologies and techniques applicable to the next-higher decade in mass (55). The NbTi solenoidal magnet (9.4 T, with dimensions 60 cm  $\times$  110 cm) was designed for exceptionally high field uniformity ( $B_r < 50$  G) to test thin-film superconducting cavities, although initially the cavities are made of electrodeposited copper (**Figure 5**). ADMX-HF (high-frequency) incorporated a dilution refrigerator from the outset, resulting in a base temperature of the experiment of  $\sim 25$  mK. Josephson parametric amplifiers (JPAs) are well suited to the initial 5-GHz range of the experiment, where they possess high gain (20–30 dB), are tunable over an octave, and can operate with  $T_N \sim T_{\text{SQL}}$  (56, 57); this noise was achieved within a factor of two in its first commissioning run. In its initial configuration, the experiment is projected to reach a sensitivity in axion–photon coupling of  $\sim 2 \times \text{KSVZ}$ .

Two promising lines of R&D are currently being pursued with high priority. The first is the prospect of incorporating type II superconducting thin films on all cylindrical surfaces of the microwave cavity to boost the  $Q$  value by an order of magnitude, to which the axion–photon conversion power and, therefore, the scanning rate are directly proportional. Xi et al. (58) recently demonstrated that a very thin film of  $\text{Nb}_x\text{Ti}_{1-x}\text{N}$  continues to exhibit RF superconductivity to frequencies  $> 100$  GHz, immersed a magnetic field parallel to its surface up to  $B_{\parallel} = 10$  T. Encouraged by this report, researchers initiated a program of making and characterizing thin (10–200-nm) NbTiN films by RF plasma deposition. They readily achieved satisfactory films on planar samples that are noncritical in exact composition (**Figure 5**). RF tests of small prototype cavities of multi-layer thin films will be conducted next, and finally the thin films will be tested in a magnetic field. Successful implementation in ADMX-HF will require minimizing lossy flux vortices penetrating the superconducting surfaces; this task requires that the films be both extremely thin and parallel to the magnetic field. To this end, the magnet was designed to meet strict specifications on field uniformity to minimize radial components.

The other major R&D effort is the incorporation of a receiver based on squeezed-vacuum states to evade the quantum limit in noise—so far employed only by the laser interferometric gravity-wave community, namely LIGO and GEO. The JILA group involved in ADMX-HF has used one

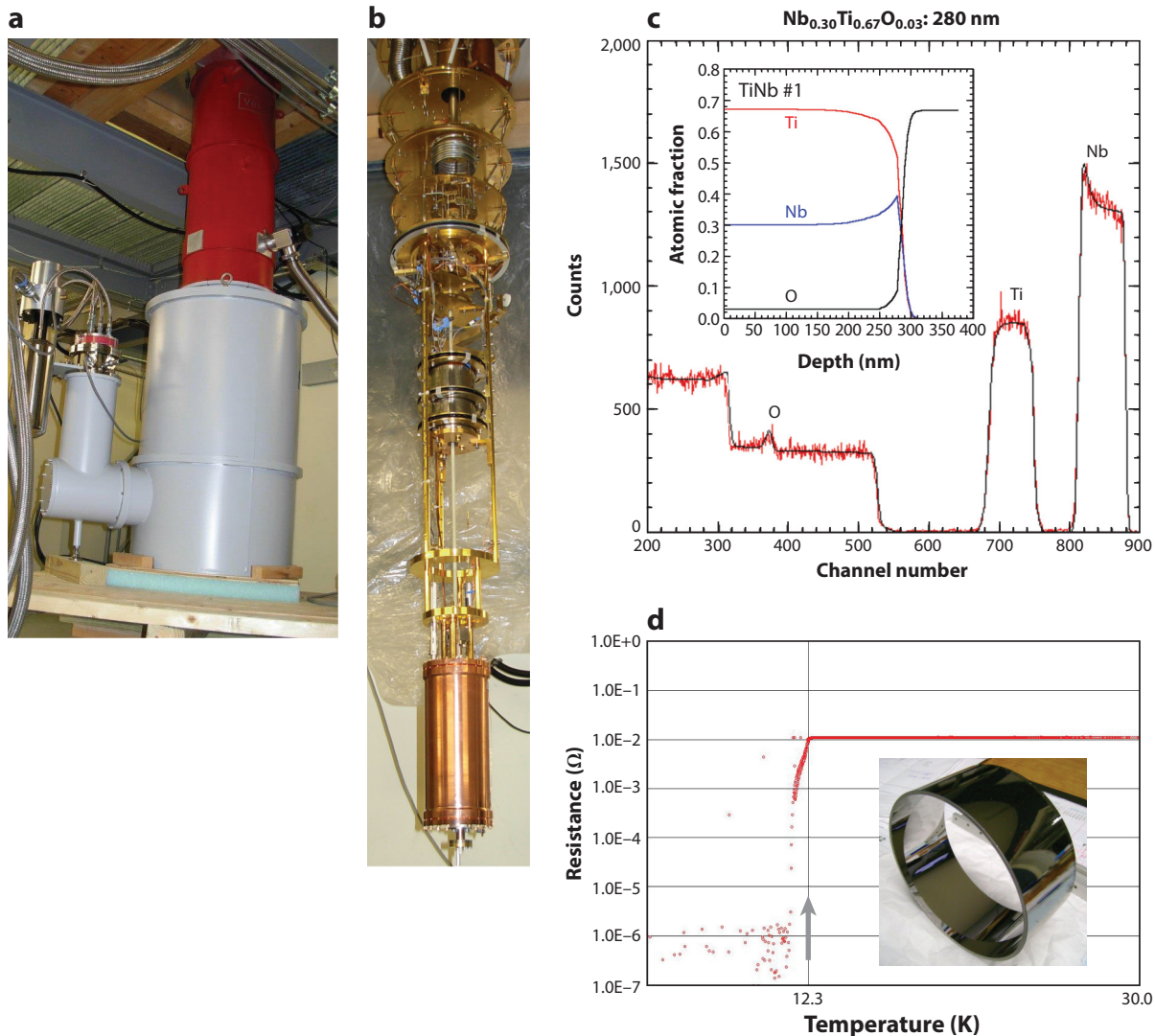


**Figure 5**

(a) ADMX-HF below deck, showing the magnet (*gray*) and dilution refrigerator (*red*). (b) Experimental gantry, showing the dilution refrigerator (*top*), the Josephson parametric amplifier’s magnetically shielded canister (*middle*), and the microwave cavity (*bottom*). (c) Rutherford backscattering profile of a thin-film superconductor. (d) Resistance versus temperature, demonstrating  $T_c > 12$  K. (*Inset*) Thin-film superconductor deposited on the inside of a 10-cm-diameter quartz tube. Panels c and d modified from Reference 54 with permission.

JPA to measure the squeezed noise generated by a second JPA (59), achieving  $T_N = b\nu/4$ . Indeed, this experiment can be considered a proof-of-principle demonstration of a quantum-noise-evading axion search. It was possible not only to measure noise in one quadrature below the SQL but also to demonstrate that the quadrature had fluctuations below vacuum because it had been squeezed. The system noise could conceivably be reduced to one-tenth of the quantum limit. Together with the gain associated with the superconducting thin-film cavity, this small-volume experiment could ultimately reach DFSZ sensitivity.

Examining quantum noise in the cavity and amplifier more rigorously, Lamoreaux et al. (60) concluded that (a) at higher frequencies and, thus, higher axion masses, single-photon detectors become competitive and ultimately favored, when compared with quantum-limited linear amplifiers, as the detector technology in the microwave cavity experiment, and (b) the crossover point in this comparison is not far above the frequencies of the current ADMX-HF search range, of order 10 GHz. The microwave cavity experiment can profitably leverage advances in superconducting qubit readout schemes (61–63).

**3.3.4. New directions and concepts.** The past few years have witnessed several new search concepts for the detection of dark matter axions. The NMR-based CASPER, designed to explore the  $10^{-6}$ – $10^{-9}$  eV mass range, is discussed separately in Section 3.4. However, other promising innovations warrant brief mention here.

Rybka et al. (64) have described an experiment designed on an open microwave resonator structure appropriate for axions in the 100–1,000- $\mu$ eV decade, where the wavelength of the microwave photon after conversion ranges from 1 to 10 mm. As the conversion probability maximizes strongly when the applied magnetic field  $B(r)$  follows the electric field of the photon mode  $E(r)$ , a wiggler-like magnetic field with a continuously tunable periodicity is required in order to sweep out the range of masses. To do so, Rybka et al. used a series of wire planes in the open resonator of alternating sign in current; ultimately, these planes will consist of superconducting wires or stripes patterned on a thin substrate. The initial prototype was able to exclude axions as dark matter between 68.2 and 76.5  $\mu$ eV, with couplings  $>4 \times 10^{-7}$  GeV $^{-1}$ —not far removed from existing limits from laser-based limits, remarkably with  $|B| < 10$  gauss. Ultimately, sensitivity to couplings of  $10^{-15}$  GeV $^{-1}$  should be achievable, below DFSZ axions for that mass range.

Sikivie et al. (65) have focused on the other challenge of the microwave cavity experiment, namely extending the search downward in mass, where, far below  $10^{-6}$  eV ( $\sim 250$  MHz), the cavity and the magnet that encloses it become unfeasibly large. To circumvent this limitation, the authors proposed replacing the cavity with a lumped-parameter LC circuit external to the magnetic field, excited by a pickup loop inside the magnet threaded by the transverse magnetic field of the mode. Optimistically, the authors represent that with a magnet such as that of the current ADMX, this technique would be maximally sensitive around  $10^{-7}$  eV, probing the band of PQ axion models. If the concept can be fully developed and implemented, such a lumped-parameter LC circuit search for dark matter axions could bridge a key gap where the cavity-based experiment and the NMR-based experiment may have difficulty overlapping.

Other new and imaginative concepts have recently been put forward. These include instrumentation of magnets of extreme aspect ratio, such as high-energy dipoles, with microwave cavities (66), as well as a proposal for a dish-geometry resonator that would be both directional and broadband in frequency (67). Such a dish antenna has already been implemented for an HP dark matter search.

### 3.4. Detection with NMR: CASPER

The CASPER proposal aims to pursue a new direction in the experimental search for axion dark matter. CASPER will detect the spin precession caused by axion dark matter by using NMR techniques (68, 69). This novel approach complements existing efforts: ADMX is sensitive to the higher axion frequencies, whereas CASPER will cover the lower frequencies, where the axion arises from energies of  $\sim 10^{15}$ – $10^{19}$  GeV.<sup>2</sup> This range is very challenging for any other technique to

---

<sup>2</sup>It used to be argued that this range was disfavored by cosmology, but that requires specific assumptions about initial conditions that are easily violated; thus, this range is allowed (see, e.g., References 70 and 71) and is also well motivated theoretically (24).

reach, although some astrophysical techniques may be able to probe it (72–74). A detection in such an experiment would not only represent the discovery of dark matter but also provide insights into the high-energy scales from which such an axion would arise, near fundamental scales such as the grand unification, Planck, or string scales.

Almost all axion experiments will search for the coupling of the axion to photons. CASPER will search for two different couplings of the axion and, thus, will naturally divide into two experiments: CASPER-Wind and CASPER-Electric. CASPER-Wind will search for the so-called axion wind effect, the direct coupling of the axion to the spin of the nucleus (69). This is the pseudoscalar coupling,

$$\mathcal{L} = \dots + g_{aNN} (\partial_\mu a) \bar{N} \gamma^\mu \gamma_5 N, \quad 20.$$

which physically causes a precession of a nucleon spin around the spatial gradient of the local axion dark matter field (69). CASPER-Electric will search for the time-varying nucleon EDM caused by the axion (68), which can be written as the coupling of the axion to nucleons:

$$\mathcal{L} = \dots - \frac{i}{2} g_d a \bar{N} \sigma_{\mu\nu} \gamma_5 N F^{\mu\nu}, \quad 21.$$

where  $F$  is the field strength of electromagnetism. This coupling arises from the fundamental defining coupling of the QCD axion to gluons  $\propto \frac{a}{f_a} G\tilde{G}$  (75). Both of these effects are time varying because the background axion dark matter field  $a$  oscillates at a frequency equal to its mass. The CASPER idea could also be used to search for the coupling of the axion to electron spin, but such a search does not seem sensitive enough to get beyond current limits in that parameter space (69). There has been a long history and significant recent interest in looking at such effects on nucleons and electrons (76–78).

The main idea behind CASPER is to use the time-varying nature of the effect (either EDM or wind) to cause precession of nuclear spins in a sample of material. The Larmor frequency of the nuclear spins is scanned by ramping the magnetic field, and at the frequency corresponding to the mass of the axion an NMR signal is observed in the usual way, by using a precise magnetometer (**Figure 6**). Many choices of possible sample material are beginning to be tested experimentally and explored theoretically (79, 80) to find the optimum.

CASPER-Wind is technically simpler than CASPER-Electric because it does not require an applied electric field and, hence, can be done using liquid xenon as the sample for which the required NMR techniques have already been perfected. It can cover large parts of general axion

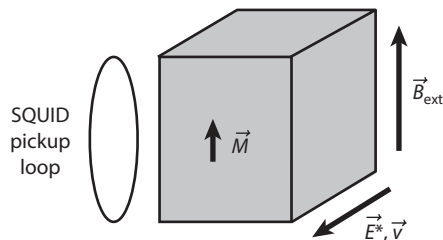


**Figure 6**

CASPER setup. The applied magnetic field  $\vec{B}_{\text{ext}}$  is colinear with the sample magnetization,  $\vec{M}$ . In CASPER-Wind the nuclear spins precess around the local velocity of the dark matter  $\vec{v}$ , whereas in CASPER-Electric the nuclear electric dipole moment causes the spins to precess around an effective electric field in the crystal  $\vec{E}^*$ , perpendicular to  $\vec{B}_{\text{ext}}$ . The superconducting quantum interference device (SQUID) pickup loop is arranged to measure the transverse magnetization of the sample.

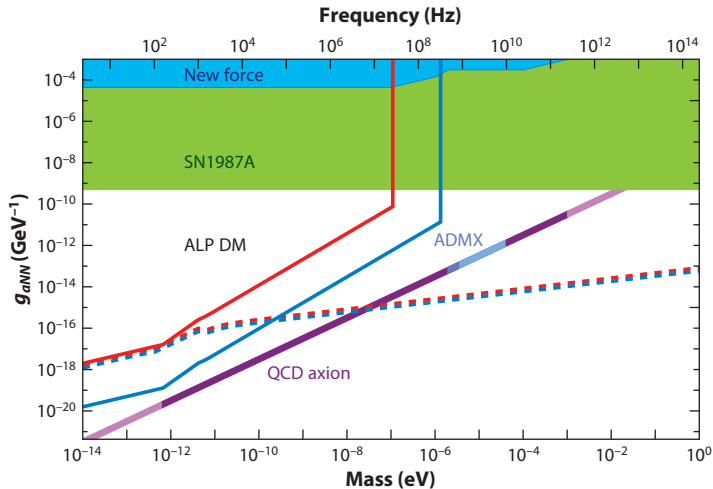


**Figure 7**

Sensitivity of the CASPER-Wind proposal. The axion-like particle (ALP) parameter space in the pseudoscalar coupling of axions to nucleons (Equation 20) is plotted versus the mass of ALPs. The purple line represents the region in which the QCD axion may lie. The width of the purple band approximates the axion model dependence in this coupling. The darker purple portion of the line shows the region in which the QCD axion could be all of the dark matter (DM) and have  $f_a < M_p$ , as in **Figure 8**. The green region is excluded by SN1987A from Reference 35. The blue region is excluded by searches for new spin-dependent forces between nuclei. The red line represents the projected sensitivity of an NMR-style experiment using xenon. The blue line represents sensitivity using  $^3\text{He}$ . The dashed lines show the limit from magnetization noise for each sample. The ADMX region shows the part of the QCD axion parameter space that has been covered (*dark blue*) (53) or will be covered in the near future (*light blue*) by ADMX. For full details, see Reference 69.

(or ALP) parameter space, many orders of magnitude beyond current constraints (**Figure 7**). It also provides a stepping stone toward CASPER-Electric; as within CASPER-Wind, many of the key technologies needed for CASPER-Electric will be developed. CASPER-Electric requires a more complicated material, such as a ferroelectric or polar crystal with a large internal electric field, but it has a better ultimate sensitivity, allowing it to reach all the way to the QCD axion over several orders of magnitude in frequency space that are unreachable by other techniques. (**Figure 8**).<sup>3</sup>

CASPER-Wind is in fact a search for any light particle that couples to nuclear spin (a generic coupling), not just the axion. For example, any pseudo-Goldstone boson is expected to possess a coupling that would be detectable by CASPER-Wind. It can also detect other types of dark matter; for example, HP dark matter (26, 88) is detectable through a nuclear dipole moment coupling.

Existing experiments may already be able to set limits on ALPs. Data from experiments searching for nuclear EDMs or investigating nucleon spin precession in a low-background environment may be reanalyzed to search for a time-varying signal, a sign of the axion. Whereas they are not ultimately as sensitive as CASPER, in which the signal is resonantly enhanced, such searches may be able to probe beyond the current astrophysical limits depicted in **Figures 7** and **8**.

CASPER is a novel and highly sensitive search for a broad class of dark matter candidates in two new parameter spaces, the axion wind and the nuclear EDM, of which the QCD axion is the

<sup>3</sup>Note that the CASPER-Wind coupling leads to a spin-dependent force that could be probed using NMR techniques as well (see, e.g., References 81–87).

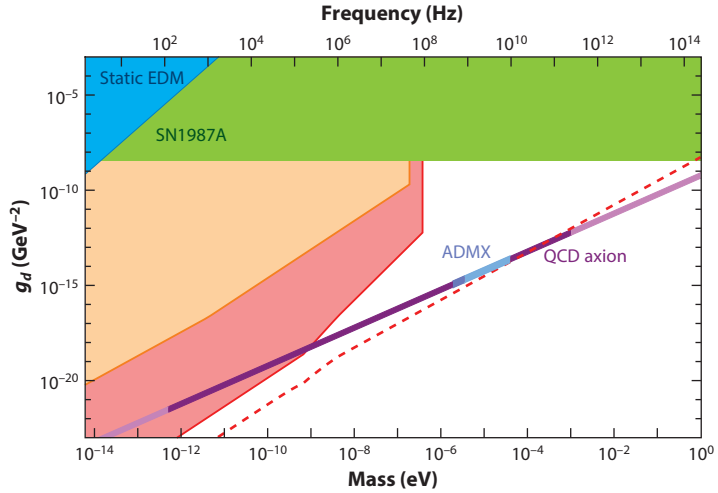


**Figure 8**

Sensitivity of the CASPER-Electric proposal. Estimated constraints in the axion-like particle (ALP) parameter space in the electric dipole moment (EDM) coupling  $g_d$  (as in Equation 21) is plotted versus the ALP mass. The blue region is excluded by existing, static nuclear EDM searches (69). The solid red and orange regions represent projected sensitivity estimates for CASPER-Electric phase 1 and 2 proposals, set by magnetometer noise. The red dashed line shows the limit from magnetization noise of the sample for phase 2. Other regions are as in Figure 7. For full details, see References 68 and 69.

best-known example. In particular, CASPER has the sensitivity to detect the QCD axion over a wide range of masses from  $\sim 10^{-9}$  eV to  $10^{-12}$  eV, which is well motivated by fundamental physics (24) and where no other experiment can detect this axion.

Construction is just beginning on CASPER. Work on CASPER is currently being carried out in several places, including Stanford University; the University of California, Berkeley; and the University of Mainz, Germany.

## 4. SEARCHES FOR SOLAR AXIONS

### 4.1. Solar Axions

Axions can be produced in the solar interior by the Primakoff conversion of plasma photons into axions in the Coulomb field of charged particles via the generic  $a\gamma\gamma$  vertex (89), giving rise to a solar axion flux at the Earth's surface (90) of  $\Phi_a = g_{10}^2 3.75 \times 10^{11} \text{ cm}^{-2} \text{ s}^{-1}$  (where  $g_{10} = g_{a\gamma\gamma}/10^{-10} \text{ GeV}^{-1}$ ). This value corresponds to a fraction of the solar luminosity of  $\mathcal{L}_a/\mathcal{L}_\odot = g_{10}^2 1.85 \times 10^{-3}$ . These axions have a broad spectral distribution around 1–10 keV, which is determined by the solar core's temperature and usefully parameterized by the following expression (Figure 9) (90):

$$\frac{d\Phi_a}{dE} = 6.02 \times 10^{10} \text{ cm}^{-2} \text{ s}^{-1} \text{ keV}^{-1} g_{10}^2 E^{2.481} e^{-E/1.205} \quad (E \text{ in keV}). \quad 22.$$

This is a robust prediction involving well-known solar physics and the generic  $a\gamma\gamma$  vertex (and thus is also valid for more generic ALPs). For particular nonhadronic axion models having a

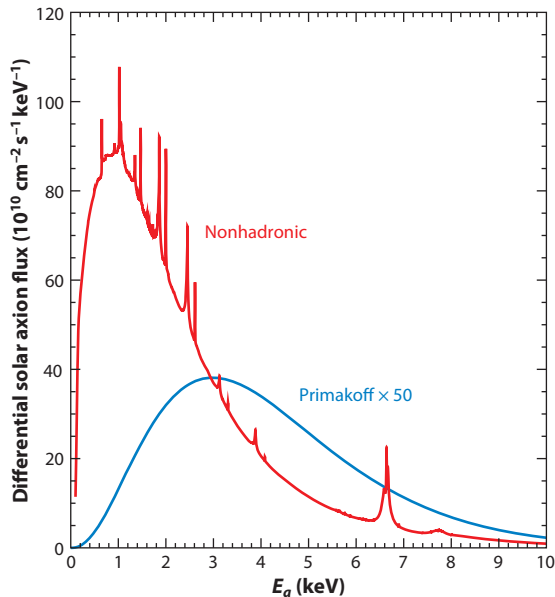


**Figure 9**

Solar axion flux due to the standard Primakoff conversion (*blue*) for  $g_{a\gamma\gamma} = 10^{-12} \text{ GeV}^{-1}$ , as well as from axion recombination, bremsstrahlung, or Compton reactions (*red*) with  $g_{aee} = 10^{-13}$ . The Primakoff spectrum has been scaled up by a factor of 50 to make both contributions comparable in the plot. Modified with permission from Reference 91.

tree-level coupling with electrons  $g_{aee}$ , other production channels, such as axion recombination, bremsstrahlung, or Compton reactions [the ABC reactions (91)] should be taken into account. As shown in **Figure 9**, if present, this additional solar axion flux could be a factor of  $\sim 10^2$  larger than the standard Primakoff one while having lower energies, peaking at  $\sim 1$  keV. However, astrophysical limits on  $g_{aee}$  are quite restrictive and largely disfavor the values that could be reached by helioscopes looking at the nonhadronic solar axion flux. In the future, the International AXion Observatory (IAXO; discussed in Section 4.4) may have sensitivity to ABC solar axions for nonexcluded values of  $g_{aee}$ . Finally, axion emission in solar nuclear transitions, by virtue of axion–nucleon interactions, has also been considered in the literature.

By means of the  $a\gamma\gamma$  vertex, solar axions can be efficiently converted back into photons in the presence of an electromagnetic field. In crystalline detectors (92–94), this effect gives rise to characteristic Bragg patterns that have been searched for as by-products of a number of underground WIMP experiments (95–99). However, the prospects of this technique have proven limited (100, 101) and do not compete with dedicated helioscope experiments that use a powerful magnet to effect the conversion. Solar axion detection by means of the axioelectric effect in the detector (102–106) or, for monochromatic axions emitted in solar nuclear transitions, the resonant absorption by the same nuclide at the detector (107–110) has also been considered. Although they are interesting for some specific WISP models, all these techniques remain far from the sensitivity required to probe QCD axion models and/or parameter space not excluded by astrophysics. So far, only axion helioscopes have reached relevant QCD axion parameter space.

---

**IAXO:** International AXion Observatory

---

## 4.2. Axion Helioscopes

The probability that an axion going through the transverse magnetic field  $B$  over a length  $L$  will convert to a photon is given by (40, 90, 111)

$$P_{a\gamma} = 2.6 \times 10^{-17} \left( \frac{B}{10 \text{ T}} \right)^2 \left( \frac{L}{10 \text{ m}} \right)^2 (g_{a\gamma\gamma} \times 10^{10} \text{ GeV})^2 F,$$

where the form factor  $F$  accounts for the coherence of the conversion process,

$$F = \frac{2(1 - \cos qL)}{(qL)^2}, \quad 23.$$

and  $q$  is the momentum transfer. The fact that the axion is not massless implies that the axion and photon states will gradually slip out of phase with distance. The coherence is preserved ( $F \simeq 1$ ) as long as  $qL \ll 1$ . For solar axion energies and a magnet length of  $\sim 10$  m, this condition is satisfied for axion masses up to  $\sim 10^{-2}$  eV, whereas for higher masses  $F$  begins to decrease, as does the sensitivity of the experiment. To mitigate the loss of coherence, a buffer gas can be introduced into the magnet beam pipes (112, 113) to impart an effective mass to the photons,  $m_\gamma = \omega_p$  (where  $\omega_p$  is the plasma frequency of the gas;  $\omega_p^2 = 4\pi\alpha n_e/m_e$ ). For axion masses that match the photon mass,  $q = 0$  and full coherence is restored. By changing the pressure of the gas inside the pipe in a controlled manner, one can systematically increase the photon mass, and the sensitivity of the experiment can be extended to higher axion masses.

The basic layout of an axion helioscope thus requires a powerful magnet coupled to one or more X-ray detectors. When the magnet is aligned with the Sun, an excess of X-rays at the exit of the magnet is expected over the background measured at nonalignment periods. This detection concept was first experimentally realized at BNL in 1992. A stationary dipole magnet with  $B = 2.2$  T and  $L = 1.8$  m was oriented toward the setting Sun (114). The experiment derived an upper limit on the axion–photon coupling of  $< 3.6 \times 10^{-9} \text{ GeV}^{-1}$  (95% CL) for masses  $< 0.03$  eV. At the University of Tokyo, a second-generation experiment was built: the SUMICO axion helioscope. Not only did this experiment implement dynamic tracking of the Sun; it also used a more powerful magnet ( $B = 4$  T,  $L = 2.3$  m) than its BNL predecessor. The bore, located between the two coils of the magnet, was evacuated, and higher-performance detectors were installed (115–117). This new setup resulted in an improved upper limit in the mass range up to 0.03 eV of  $< 6.0 \times 10^{-10} \text{ GeV}^{-1}$  (95% CL). Later experimental improvements included the additional use of a buffer gas to enhance sensitivity to higher-mass axions.

## 4.3. CAST

A third-generation experiment, CAST, began data collection in 2003 and is still in operation. The experiment uses an LHC dipole prototype magnet with a magnetic field of up to 9 T over a length of 9.3 m (118). CAST is able to follow the Sun for several hours per day by using an elevation and azimuth drive. This CERN experiment is the first helioscope to employ X-ray focusing optics for one of its four detector lines (119), as well as low-background techniques from detectors in underground laboratories (120–122). During its observational program from 2003 to 2011, CAST operated first with its magnet bores under vacuum (2003–2004) to probe masses  $< 0.02$  eV. No significant signal above background was observed. Thus, an upper limit on the axion–photon coupling of  $< 8.8 \times 10^{-11} \text{ GeV}^{-1}$  (95% CL) was obtained (90, 111). The experiment was then upgraded to be operated with  $^4\text{He}$  gas (2005–2006) and  $^3\text{He}$  gas (2008–2011) to obtain continuous high sensitivity up to an axion mass of 1.17 eV. Data released up to now provide average limits on  $g_{a\gamma\gamma}$  of  $\lesssim 2.3 \times 10^{-10} \text{ GeV}^{-1}$  (95% CL) for the higher mass range  $0.02 \text{ eV} < m_a < 0.64 \text{ eV}$

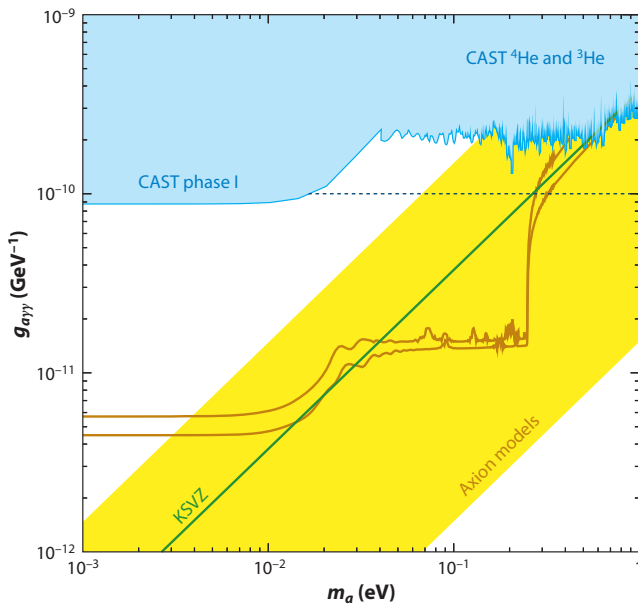


**Figure 10**

Axion-like particle parameter space ( $g_{a\gamma\gamma} - m_a$ ), showing the region (yellow band) where QCD axion models lie. Solid areas indicate the regions excluded by current experiments, among them CAST, and the two brown lines represent the expected sensitivity of the future IAXO under two different sets of assumptions.

(113, 123), and of  $\lesssim 3.3 \times 10^{-10} \text{ GeV}^{-1}$  (95% CL) for the mass range  $0.64 \text{ eV} < m_a < 1.17 \text{ eV}$  (124); the exact value depends on the pressure setting. The envelope of all these limits is shown in **Figure 10**. By-products of CAST include the search for 14.4-keV solar axions emitted in the M1 transition of  $^{57}\text{Fe}$  nuclei (125); the search for MeV axions from  $^7\text{Li}$  and  $\text{D}(p, \gamma)^3\text{He}$  nuclear transitions (126); the search for solar axions from ABC reactions (127); and the search of more exotic ALP or WISP models, such as chameleon particles also potentially emitted in the Sun (128, 129). As part of the R&D to assess the technologies for the next-generation axion helioscope IAXO, new lower-background Micromegas (micromesh gaseous structure) detectors are actively being developed (121, 122), and a new X-ray telescope coupled with one such detector was built and installed in CAST in 2014. This improved equipment is currently allowing CAST to revisit the  $^4\text{He}$  (in 2012) and vacuum (in 2013–2015) configurations with an incremental improvement in sensitivity.

So far, each subsequent generation of axion helioscopes has resulted in an improvement in sensitivity to the axion–photon coupling constant of approximately a factor of six over its predecessors. CAST has been the first axion helioscope to surpass the stringent limits from astrophysics ( $g_{a\gamma\gamma} \lesssim 10^{-10} \text{ GeV}^{-1}$ ) over a large mass range and to probe allowed ALP parameter space. As shown in **Figure 10**, in the region of higher axion masses ( $m_a \gtrsim 0.1 \text{ eV}$ ), the experiment has entered the band of QCD axion models for the first time and has excluded KSVZ axions of specific mass values. CAST is the largest collaboration in axion physics, with  $\sim 70$  physicists from  $\sim 16$  different institutions in Europe and the United States. The scalability of the helioscope technique has recently been proven (130), and a substantial step beyond the CAST state of the art could be achieved with the proposed IAXO.

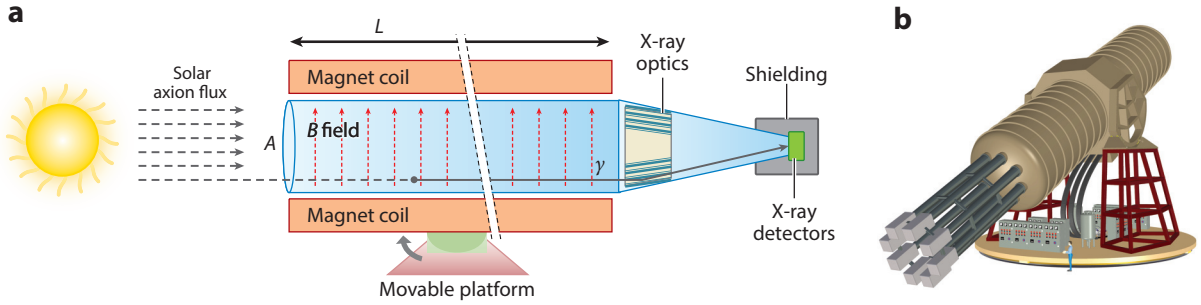


**Figure 11**

(a) Conceptual arrangement of an enhanced axion helioscope with X-ray focusing. Solar axions are converted into photons by the transverse magnetic field inside the bore of a powerful magnet. The resulting quasi-parallel beam of photons of cross-sectional area  $A$  is concentrated by appropriate X-ray optics onto a small spot area  $a$  in a low-background detector. (b) The envisaged design for IAXO includes eight such magnet bores, depicted with their respective optics and detectors. Modified with permission from Reference 130.

#### 4.4. IAXO

Significant improvement over CAST sensitivity is possible only by utilizing a new magnet, designed and built to maximize the helioscope magnet's figure of merit,  $f_M = B^2 L^2 A$  (where  $B$ ,  $L$ , and  $A$  are the magnet's field strength, length, and cross-sectional area, respectively), which is proportional to the photon signal from converted axions (130). However, for this figure of merit to directly translate into the signal-to-noise ratio of the overall experiment for a large-aperture magnet, the entire cross-sectional area of the magnet must be equipped with X-ray focusing optics. The layout of this enhanced axion helioscope (**Figure 11**) was proposed (130) as the basis for IAXO. The conceptual design of this project was recently finished (131), and the technical design report, including some prototyping activities, is in preparation. A recent Letter of Intent (132) to CERN was positively reviewed.

The goals of producing an intense magnetic field over a large volume and maximizing the figure of merit within realistic limits of the different technologies motivate the move to a 25-m-long, 5.2-m-diameter toroid assembled from eight coils, producing 2.5 T in eight 600-mm-diameter bores (133). The magnet is supported by a tracking system similar to that of large telescopes. **Figure 11** shows the conceptual design of the infrastructure (131). Each of the bores will be equipped with X-ray optics similar to those used on NASA's NuSTAR (134), an X-ray astrophysics satellite with two focusing telescopes that operate in the 3–79-keV band, consisting of thousands of thermally formed glass substrates deposited with multilayer coatings. For IAXO, the multilayer coatings will be designed to match the solar axion spectrum (135). At the focal plane in each of the optics, IAXO will have small gaseous chambers read by pixelated planes of Micromegas, surrounded by active and passive shielding. These detectors are being developed (136–138; <http://gifna.unizar.es/trex/>) for rare event searches, and they have the potential to reach background levels below  $\sim 10^{-7}$  counts  $\text{keV}^{-1} \text{cm}^{-2} \text{s}^{-1}$  in IAXO (121, 122). These levels are achieved by the use of radiopure detector components, shielding, and offline discrimination algorithms on the three-dimensional event topology in the gas registered by the pixelated readout.

IAXO will have a signal-to-noise ratio that is five orders of magnitude better than that of CAST, which means a sensitivity to both  $g_{a\gamma\gamma}$  values as low as, or even surpassing,  $\sim 5 \times 10^{-12} \text{ GeV}^{-1}$ , for a wide range of axion masses up to  $\sim 0.01 \text{ eV}$  after  $\sim 3$  years of data taking in vacuum, and  $g_{a\gamma\gamma}$  values from  $\sim 10^{-11} \text{ GeV}^{-1}$  up to  $\sim 0.25 \text{ eV}$ , after an additional  $\sim 3$  years with the use of a buffer gas in the conversion bores. IAXO will thus enter deeply into unexplored ALP and axion parameter space (**Figure 10**). At the lowest mass values, IAXO will test ALP models invoked to explain the anomalies in light propagation over astronomical distances. At the high mass values ( $>1 \text{ meV}$ ), IAXO will explore a broad range of QCD axion models. Its sensitivity would reach axion models with masses down to the few meV range, superseding the SN1987A energy loss limits on the axion mass and entering parameter space of progressively higher cosmological interest. At the higher mass values ( $0.1\text{--}1 \text{ eV}$ ), axions are good candidates to the hot DM or additional dark radiation that could restore agreement in cosmological parameters. IAXO could also be sensitive to ABC solar axions for nonexcluded values of  $g_{aee}$  and thus directly test the models invoked to solve the anomalous cooling observed for white dwarfs (38, 139, 140). Additional equipment beyond the baseline configuration [such as InGrid detectors, transition edge sensors, or low-noise charge-coupled devices (CCDs) (132)] would extend the detection energy window, enabling exploration of other, less standard physics cases (e.g., the possibility to directly detect the cosmic axion background predicted by some dark radiation models). Finally, the possibility of equipping the huge magnetic volume of IAXO with microwave cavities or antennae sensitive to relic axions is being studied, with promising preliminary projections (141) in mass ranges complementary to those of previous haloscope searches.

## 5. PURELY LABORATORY EXPERIMENTS

In recent years, there has been increasing interest in experiments searching for axions or other light exotica that do not rely on cosmological or astrophysical sources. This section concerns photon regeneration, colloquially referred to as light shining through walls (LSW), by which photons mix with axions (or WISPs more generally); the axions (or WISPs) are regenerated into the photon state on the other side of an optical barrier (**Figure 12**). For axions, production and regeneration require a transverse magnetic field, but magnets may or may not be required for WISPs in general. We do not attempt to cover the sector of short-range spin dependent forces, which would require a review of its own.

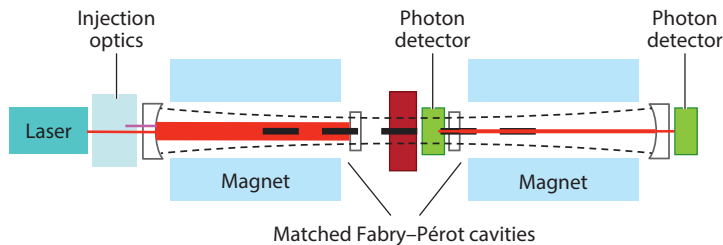


**Figure 12**

The principle of photon regeneration. Current and future experiments will employ Fabry–Pérot cavities, for both the production and regeneration regions and actively locked together, to greatly enhance the experimental sensitivity. The ALPS I experiment has already used such a cavity in its production region (142, 143).

The most sensitive LSW experiments today use or plan to use coherent light to provide the photons before the wall. Such light offers the possibility to enhance sensitivities by implementing Fabry–Pérot cavities (**Figure 12**):

1. A cavity in front of the wall enables one to recycle the light shining against the wall and, hence, to increase the effective light power by a power-buildup factor  $\mathcal{F}_{\text{PC}}$  (where PC stands for production cavity).
2. A cavity with a power-buildup factor  $\mathcal{F}_{\text{RC}}$  (where RC stands for regeneration cavity) behind the wall increases the reconversion probability. This technique is called resonant regeneration.<sup>4</sup>

The influence of the empty cavity behind the wall is similar to the Purcell effect, first described in 1946 (144; also see References 145 and 146 for related experiments). The implementation of resonating cavities in LSW experiments has been worked out in more detail elsewhere (147–149). Given that  $\mathcal{F}$  factors of several  $10^4$  in the optical regime and even several  $10^5$  for microwaves can be reached, resonators enable significant improvements in experimental sensitivity.

### 5.1. Light-Shining-Through-Walls Experiments with Microwaves, Optical Photons, and X-Rays

Experiments using microwaves usually work in the near-field approximation. One can picture this situation as having a PC emitting a beam of WISPs whose shape is determined by the mode resonating in the cavity. Thus, one has to place the RC, or detector cavity, somewhere next to the PC so that WISPs pass through it. The probability of a photon–WISP–photon oscillation ( $\gamma \rightarrow \phi \rightarrow \gamma$ ) with an effective photon–WISP coupling  $C_{\text{WISP}}$  in such an installation (150, 151) is given by Equation 24, where the geometrical form factor  $G$  describes the overlap of the modes resonating in the PC and RC. The size of such experiments is essentially given by the microwave wavelength:

$$P_{\gamma \rightarrow \phi \rightarrow \gamma} = |C_{\text{WISP}}|^4 \cdot |G|^2 \cdot \mathcal{F}_{\text{PC}} \cdot \mathcal{F}_{\text{RC}}. \quad 24.$$

In a far-field approximation (as realized with optical photons and X-rays), the conversion probability is given by

$$P_{\gamma \rightarrow \phi \rightarrow \gamma} = \frac{\omega}{\sqrt{\omega^2 - m_\phi^2}} \cdot |C_{\text{WISP}}|^4 \cdot \mathcal{F}_{\text{PC}} \cdot \mathcal{F}_{\text{RC}} \cdot \sin^4 \left( \frac{q \cdot l}{2} \right). \quad 25.$$

Here,  $q = |n \cdot \omega - \sqrt{\omega^2 - m_\phi^2}|$ ;  $\omega$  is the photon energy,  $m_\phi$  is the WISP mass,  $n$  is the refractive index, and  $l$  is the length of the experiment in front of and behind the wall. For HPs and ALPs, the couplings are given by

$$|C_{\text{HP}}|^2 = 4\chi^2 \cdot \frac{m_\phi^4}{(m_\phi^2 + 2\omega^2(n-1))^2}; \quad |C_{\text{ALP}}|^2 = 4 \cdot \frac{(g_{a\gamma\gamma}\omega B)^2}{(m_\phi^2 + 2\omega^2(n-1))^2}, \quad 26.$$

where  $\chi$  is a dimensionless parameter and  $g_{a\gamma\gamma}$  is the two-photon coupling strength with dimension  $\text{mass}^{-1}$ . In Equation 26, the homogeneous magnetic field is assumed to be oriented perpendicular (parallel) to the electric field of the light wave for interaction with scalar (pseudoscalar) ALPs.

<sup>4</sup>The factor  $\mathcal{F}$  is in fact the finesse of the Fabry–Pérot resonator. The quality factor  $Q$  of the resonator, which determines the intrinsic line width, is given by  $Q = (l/\lambda)\mathcal{F}$ , where  $l$  is the length of the cavity and  $\lambda$  is the wavelength.

The maximal sensitivity is obtained in vacuum with  $n = 1$ . Following Equations 25 and 26, one arrives at the following approximation for  $ql \ll 1$  and  $n = 1$ :

$$P_{\gamma \rightarrow \phi \rightarrow \gamma} = \frac{1}{16} \cdot \mathcal{F}_{\text{PC}} \mathcal{F}_{\text{RC}} \cdot (g_{a\gamma\gamma} Bl)^4 = 6 \cdot 10^{-38} \cdot \mathcal{F}_{\text{PC}} \mathcal{F}_{\text{RC}} \cdot \left( \frac{g_{a\gamma\gamma}}{10^{-10} \text{ GeV}^{-1}} \frac{B}{1 \text{ T}} \frac{l}{10 \text{ m}} \right)^4. \quad 27.$$

The leading microwave LSW experiment is the CERN Resonant Weakly Interacting sub-eV Particle Search (CROWS) (152). CROWS has fully exploited the resonant regeneration technique described above and has achieved about the same sensitivity as the optical experiments ALPS I at DESY (142) and OSQAR at CERN (153), which had no cavity behind the wall. ALP–photon couplings around  $g_{a\gamma\gamma} = 5 \times 10^{-8} \text{ GeV}^{-1}$  have been probed. Whereas CROWS has searched for ALPs up to its kinematic limit,  $m_\phi = \omega$ , the optical experiments were limited to roughly  $m_\phi < 10^{-3} \omega$  due to Equation 25.

LSW experiments have also been performed with intense X-ray beams available at synchrotron radiation sources (154, 155). Due to the higher photon energy, such experiments can probe WISPs up to eV masses and beyond, but due to the relatively low photon number flux and the present impossibility of implementing cavities with high power buildups, X-ray-based experiments do not reach the sensitivity of optical or microwave LSW experiments.

## 5.2. The Future of Light-Shining-Through-Walls Experiments

The most advanced proposal is the ALPS II (156) project, which is in preparation at DESY (**Figure 13**). **Table 1** compares critical parameters of ALPS I, ALPS II, and a future experiment, JURA (Joint Undertaking on Research for Axion-like particles). Evidently, ALPS II has the potential to increase the sensitivity for  $g_{a\gamma\gamma}$  by more than three orders of magnitude, reaching down to  $g_{a\gamma\gamma} = 2 \times 10^{-11} \text{ GeV}^{-1}$  and thereby going beyond present-day limits from astrophysics.

To realize an experiment such as that shown in **Figures 12** and **13**, both cavities must be mode matched and phase locked. At ALPS II, continuous-wave IR light (1,064 nm) with a power of up to 35 W is provided by a single-mode, single-frequency laser system. Through a curved mirror, the laser light is injected into the cavity in front of the wall, which is locked via the Pound–Drever–Hall (PDH) sensing scheme (157). The ALPS II cavity is designed for an  $\mathcal{F}_{\text{RC}}$  value of 5,000, providing a circulating power of 150 kW and limiting the power density on the mirrors to  $500 \text{ kW cm}^{-2}$ , approximately an order of magnitude below their damage thresholds. For the cavity to be locked behind the wall with the PDH method, a fraction of the 1,064-nm light is frequency doubled to 532 nm in a KTP crystal and fed into the cavity target for an  $\mathcal{F}_{\text{RC}}$  value of 40,000. For future experiments beyond ALPS II, one might increase the circulating light power in front of the wall by another order of magnitude (also see Reference 149) and improve on the  $\mathcal{F}_{\text{RC}}$  value by use of advanced seismic isolation of the optical components, for example.

ALPS II will use a transition edge sensor (158, 159) based on a thin superconducting tungsten film ( $25 \mu\text{m} \times 25 \mu\text{m} \times 20 \text{ nm}$ ) for the photon detectors. Photons with a wavelength of 1,064 nm appear as fast pulses with a decay time of approximately 1.5  $\mu\text{s}$ . The intrinsic background is below  $10^{-4} \text{ counts s}^{-1}$ , the energy resolution for single IR photons is better than 10%, and the whole system can be operated stably over long timescales (160–162). IR photon detection sensitivity well below megahertz rates should be achievable.

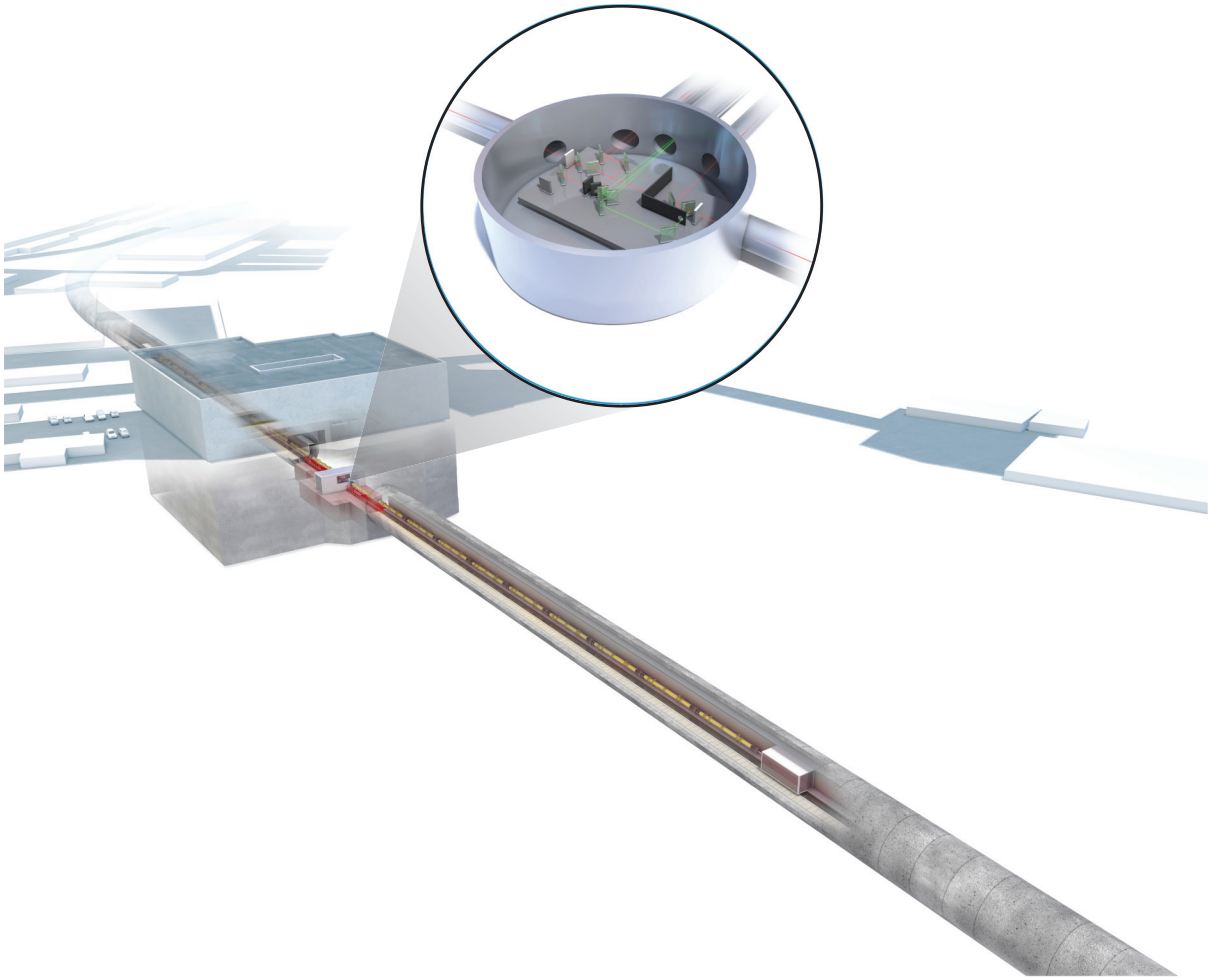


**Figure 13**

An artist's view of the ALPS II experiment under preparation at DESY. A string of 20 HERA dipole magnets is planned to be installed in a straight section of the tunnel of the decommissioned HERA accelerator. (*Inset*) Parts of the central optics used to align and control the two optical resonators in front of and behind the wall. Modified with permission from Reference 156. Copyright 2013, DESY.

An alternative detection scheme has been proposed (149) in which the regeneration cavity is controlled by light whose frequency is shifted by only a few free spectral ranges, compared with the light in the production cavity (not frequency doubled as for ALPS II). This approach would allow one to carry out a heterodyne detection of the reconverted photons behind the wall by mixing their signal (which would occur at the PC's light frequency) with the light controlling the regeneration cavity. In principle, any detector background noise can be rendered negligible in this scheme.

The coupling  $g_{a\gamma\gamma}$  that can be reached goes as  $(Bl)^{-1}$ , but at present LSW experiments have used only one or two dipole magnets. The maximal length of an LSW experiment depends on the aperture of the magnets and the laser beam divergence. This restriction limits the ALPS II setup to

**Table 1** Comparison between parameters of the ALPS I (142) and ALPS II (156) experiments and those of a hypothetical future experiment, JURA

Parameter	Sensitivity <sup>a</sup>	ALPS I	ALPS II	JURA
Effective laser power $P_{\text{LASER}}$	$g_{a\gamma\gamma} \propto P_{\text{LASER}}^{-1/4}$	1 kW	150 kW	1,000 kW
$\mathcal{F}_{\text{RC}}$	$g_{a\gamma\gamma} \propto \mathcal{F}_{\text{RC}}^{-1/4}$	1	40,000	100,000
Length ( $B$ field) $l$	$g_{a\gamma\gamma} \propto (l)^{-1}$	4.4 m	88 m	286 m
Magnetic field $B$	$g_{a\gamma\gamma} \propto (B)^{-1}$	5.0 T	5.3 T	13 T

<sup>a</sup>The second column shows the dependence of the reachable ALP–photon coupling on the experimental parameters. Abbreviation: ALP, axion-like particle.

a total length of approximately 200 m, for example, which represents 20 HERA dipole magnets.<sup>5</sup> In the far future, one can imagine magnet strings based on the dipoles under development at CERN (163, 164), which will offer a field of approximately 13 T with an aperture of approximately 100 mm if the high-critical-temperature ( $T_c$ ) superconducting inner part is removed (see the JURA<sup>6</sup> entry in **Table 1**).

The next generation of laser-based LSW experiments, such as ALPS II, will surpass present limits on ALPs from astrophysics observations and will have the potential to probe a large fraction of the parameter space for ALPs, as indicated by the cooling of stars or the abnormally high transparency of the Universe for TeV photons. However, at present no concept exists for how to access the QCD axion with purely laboratory-based experiments. Only once the axion mass is known from dark matter experiments, for example, can one consider optimizing the sensitivity of LSW experiments accordingly (165).

## 6. SUMMARY AND CONCLUSIONS

**Figure 14** schematically represents the current limits on the photon coupling of axions and ALPs, as well as the projected extension of these results with ongoing upgrades within the next 5 years; **Figures 7** and **8** summarize the reach of future NMR experiments for lower-mass axions through their nucleon coupling. Along with experiments still in the conceptual or prototype phase, these experiments constitute, for the first time, the emergence of a complete strategy to definitively answer the question of the existence of the axion, and its cosmological role, from the neV-to-meV mass range. Interestingly, it has been the mass coverage rate, not the sensitivity of all dark matter axion searches, that has been the limiting factor. If the mass were known, virtually any microwave cavity experiment would be able to detect the axion with sufficient integration time. In fact, if the axion were discovered, it would quickly become a senior undergraduate physics laboratory experiment. The heart of the issue with tuning high- $Q$  experiments is that their exquisite sensitivity accrues as a trade-off for spectral bandwidth, thus necessitating tuning over a decade or more of mass.

The searches for ALPs based on axion–photon mixing in the relativistic limit, namely helioscope and LSW experiments, have also achieved an impressive technical sophistication and are now poised for a dramatic scale-up from earlier realizations. Whereas their ultimate projections in  $g_{a\gamma\gamma}$  might improve on the best astrophysical limits by only an order of magnitude or so, these

<sup>5</sup>The dipole magnets will be straightened to provide a sufficient aperture.

<sup>6</sup>Using 532-nm light instead of 1,064-nm light would enable a further doubling of the length.

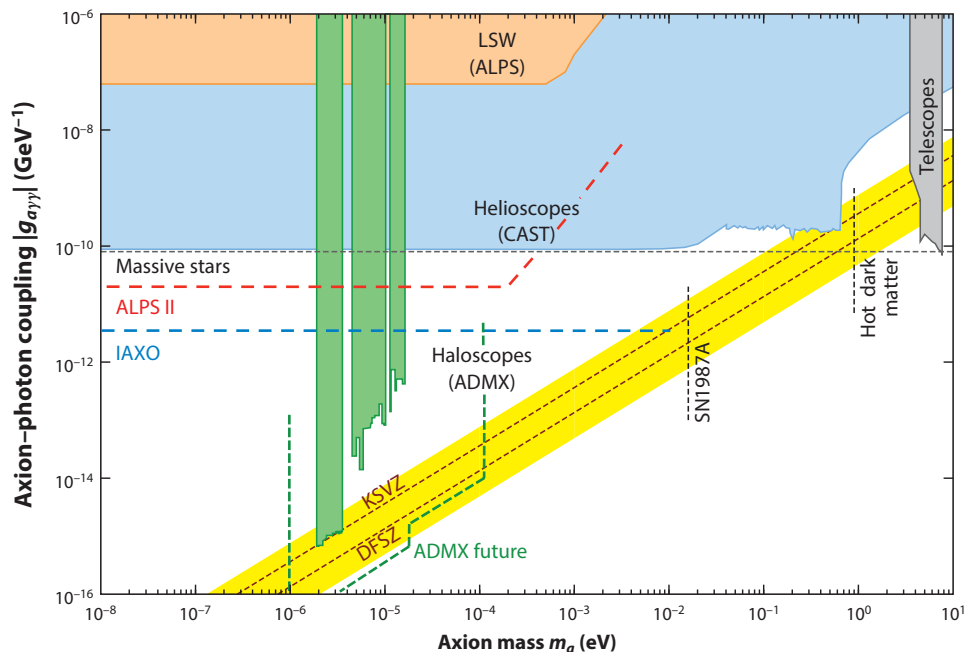


**Figure 14**

Existing limits on the photon coupling of axions and axion-like particles and the projected coverage of ongoing upgrades for these experiments. Abbreviation: LSW, light shining through walls. Modified with permission from Reference 39. Copyright 2014, Particle Data Group.

experiments are extremely important insofar as they have discovery potential for generalized pseudoscalars that may have no origin in PQ symmetry, and for which the microwave cavity experiments would be irrelevant. We are hopeful, even optimistic, that the next major review will focus on the properties of the already-discovered axion and the new field of axion astronomy and cosmology.

## DISCLOSURE STATEMENT

The authors are not aware of any affiliations, memberships, funding, or financial holdings that might be perceived as affecting the objectivity of this review.

## ACKNOWLEDGMENTS

P.W.G. acknowledges support from National Science Foundation grant PHY-1316706, US Department of Energy Early Career Award DE-SC0012012, and the Terman Fellowship. I.G.I. acknowledges support from the Spanish Ministry of Economy and Competitiveness (MINECO) under contracts FPA2011-24058, FPA2013-41085, and CSD2007-00042 (CPAN project), as well as from the European Research Council under T-REX Starting Grant ERC-2009-StG-240054 of the IDEAS program of the Seventh EU Framework Program. S.K.L. and K.v.B. acknowledge support from the National Science Foundation under grants PHY-1067242 and PHY-1306729, respectively. We thank J.A. Garcia for help with **Figure 9**.

## LITERATURE CITED

1. Weinberg S. *Phys. Rev. Lett.* 40:223 (1978)
2. Wilczek F. *Phys. Rev. Lett.* 40:279 (1978)
3. Peccei R, Quinn HR. *Phys. Rev. Lett.* 38:1440 (1977)
4. Peccei R, Quinn HR. *Phys. Rev. D* 16:1791 (1977)
5. Asztalos SJ, et al. *Annu. Rev. Nucl. Part. Sci.* 56:293 (2006)
6. Rosenberg L, van Bibber K. *Phys. Rep.* 325:1 (2000)
7. Bradley R, et al. *Rev. Mod. Phys.* 75:777 (2003)
8. Kim JE. *Phys. Rep.* 150:1 (1987)
9. Cheng HY. *Phys. Rep.* 158:1 (1988)
10. Turner MS. *Phys. Rep.* 197:67 (1990)
11. Raffelt GG. *Phys. Rep.* 198:1 (1990)
12. Kim JE, Carosi G. *Rev. Mod. Phys.* 82:557 (2010)
13. Khriplovich I, Lamoreaux S. *CP Violation Without Strangeness—Electric Dipole Moments of Particles, Atoms, and Molecules* (1997). Berlin: Springer
14. Landau L, Lifshitz E. In *Course of Theoretical Physics*, vol. 2. Oxford, UK: Butterworth-Heinemann (1975)
15. Baluni V. *Phys. Rev. D* 19:2227 (1979)
16. Crewther R, Vecchia PD, Veneziano G, Witten E. *Phys. Lett. B* 88:123 (1979); Crewther R, Vecchia PD, Veneziano G, Witten E. Erratum. *Phys. Lett. B* 91:487(E) (1980)
17. Baker C, et al. *Phys. Rev. Lett.* 97:131801 (2006)
18. Ellis J, Gaillard MK. *Nucl. Phys. B* 150:141 (1979)
19. Khriplovich I, Vainshtein A. *Nucl. Phys. B* 414:27 (1994)
20. Kim JE. *Phys. Rev. Lett.* 43:103 (1979)
21. Shifman MA, Vainshtein A, Zakharov VI. *Nucl. Phys. B* 166:493 (1980)
22. Dine M, Fischler W, Srednicki M. *Phys. Lett. B* 104:199 (1981)
23. Zhitnitsky A. *Sov. J. Nucl. Phys.* 31:260 (1980)
24. Svrček P, Witten E. *J. High Energy Phys.* 0606:051 (2006)
25. Jaeckel J, Ringwald A. *Annu. Rev. Nucl. Part. Sci.* 60:405 (2010)
26. Arias P, et al. *J. Cosmol. Astropart. Phys.* 1206:013 (2012)
27. Ringwald A. *Phys. Dark Universe* 1:116 (2012)
28. Meyer M, Horns D, Raue M. *Phys. Rev. D* 87:035027 (2013)
29. Rubtsov G, Troitsky S. *JETP Lett.* 100:397 (2014)
30. Ayala A, et al. *Phys. Rev. Lett.* 113:191302 (2014)
31. Miller Bertolami MM, Melendez BE, Althaus LG, Isern J. *J. Cosmol. Astropart. Phys.* 1410:069 (2014)
32. Altarelli G. *Nucl. Instrum. Methods A* 742:56 (2014)
33. Feng JL. *Annu. Rev. Nucl. Part. Sci.* 63:351 (2013)
34. Sikivie P. *Lect. Notes Phys.* 741:19 (2008)
35. Raffelt GG. *Lect. Notes Phys.* 741:51 (2008)
36. Isern J, Garcia-Berro E, Torres S, Catalan S. *Astrophys. J. Lett.* 682:109 (2008)
37. Isern J, Garcia-Berro E, Althaus L, Corsico A. *Astron. Astrophys.* 512:A86 (2010)
38. Corsico A, et al. *J. Cosmol. Astropart. Phys.* 1212:010 (2012)
39. Olive K, et al. *Chin. Phys. C* 38:090001 (2014)
40. Sikivie P. *Phys. Rev. Lett.* 51:1415 (1983)
41. Sikivie P. *Phys. Rev. D* 32:2988 (1985)
42. Dicke R. *Rev. Sci. Instrum.* 17:268 (1946)
43. Sikivie P. *Phys. Lett. B* 695:22 (2011)
44. van Bibber K, Kinion S. *Philos. Trans. R. Soc. Lond. A* 361:2553 (2003)
45. De Panfilis S, et al. *Phys. Rev. Lett.* 59:839 (1987)
46. Wuensch W, et al. *Phys. Rev. D* 40:3153 (1989)
47. Hagemann C, Sikivie P, Sullivan N, Tanner D. *Phys. Rev. D* 42:1297 (1990)
48. Tada M, et al. *Phys. Lett. A* 349:488 (2006)
49. Mück M, et al. *Appl. Phys. Lett.* 72:2885 (1998)

50. Mück M, et al. *Appl. Phys. Lett.* 75:3545 (1999)
51. Mück M, Clarke J. *J. Appl. Phys.* 88:6910 (2000)
52. Kinion D, Clarke J. *Appl. Phys. Lett.* 98:202503 (2011)
53. Asztalos S, et al. *Phys. Rev. Lett.* 104:041301 (2010)
54. Hoskins J, et al. *Phys. Rev. D* 84:121302 (2011)
55. Shokair T, et al. *Int. J. Mod. Phys. A* 29:1443004 (2014)
56. Castellanos-Beltran MA, Lehnert KW. *Appl. Phys. Lett.* 91:083509 (2007)
57. Castellanos-Beltran MA, et al. *Nat. Phys.* 4:929 (2008)
58. Xi X, et al. *Phys. Rev. Lett.* 105:257006 (2010)
59. Mallet F, et al. *Phys. Rev. Lett.* 106:220502 (2011)
60. Lamoreaux S, van Bibber K, Lehnert K, Carosi G. *Phys. Rev. D* 88:035020 (2013)
61. Schuster DI, et al. *Nature* 445:515 (2007)
62. Wallraff A, et al. *Nature* 431:162 (2004)
63. Chen YF, et al. *Phys. Rev. Lett.* 107:217401 (2011)
64. Rybka G, Wagner A. arXiv:1403.3121 [physics.ins-det] (2014)
65. Sikivie P, Sullivan N, Tanner D. *Phys. Rev. Lett.* 112:131301 (2014)
66. Baker OK, et al. *Phys. Rev. D* 85:035018 (2012)
67. Horns D, et al. *J. Cosmol. Astropart. Phys.* 1304:016 (2013)
68. Budker D, et al. *Phys. Rev. X* 4:021030 (2014)
69. Graham PW, Rajendran S. *Phys. Rev. D* 88:035023 (2013)
70. Linde AD. *Phys. Lett. B* 201:437 (1988)
71. Wilczek F. arXiv:1204.4683 [hep-th] (2012)
72. Arvanitaki A, Baryakhtar M, Huang X. arXiv:1411.2263 [hep-ph] (2014)
73. Arvanitaki A, Dubovsky S. *Phys. Rev. D* 83:044026 (2011)
74. Arvanitaki A, et al. *Phys. Rev. D* 81:123530 (2010)
75. Graham PW, Rajendran S. *Phys. Rev. D* 84:055013 (2011)
76. Stadnik Y, Flambaum V. *Phys. Rev. D* 89:043522 (2014)
77. Stadnik YV, Flambaum VV. arXiv:1409.2986 [hep-ph] (2014)
78. Hong J, Kim JE. *Phys. Lett.* B265:197 (1991)
79. Roberts B, et al. *Phys. Rev. D* 90:096005 (2014)
80. Roberts B, et al. *Phys. Rev. Lett.* 113:081601 (2014)
81. Moody J, Wilczek F. *Phys. Rev. D* 30:130 (1984)
82. Vasilakis G, Brown J, Kornack T, Romalis M. *Phys. Rev. Lett.* 103:261801 (2009)
83. Burghoff M, et al. *J. Phys. Conf. Ser.* 295:012017 (2011)
84. Ledbetter M, Romalis M, Jackson-Kimball D. *Phys. Rev. Lett.* 110:040402 (2013)
85. Heil W, et al. *Annalen Phys.* 525:539 (2013)
86. Tullney K, et al. *Phys. Rev. Lett.* 111:100801 (2013)
87. Arvanitaki A, Geraci AA. *Phys. Rev. Lett.* 113:161801 (2014)
88. Nelson AE, Scholtz J. *Phys. Rev. D* 84:103501 (2011)
89. Raffelt GG. *Annu. Rev. Nucl. Part. Sci.* 49:163 (1999)
90. Andriamonje S, et al. *J. Cosmol. Astropart. Phys.* 0704:010 (2007)
91. Redondo J. *J. Cosmol. Astropart. Phys.* 1312:008 (2013)
92. Buchmüller W, Hoogeveen F. *Phys. Lett. B* 237:278 (1990)
93. Paschos EA, Zioutas K. *Phys. Lett. B* 323:367 (1994)
94. Creswick RJ, et al. *Phys. Lett. B* 427:235 (1998)
95. Avignone FTI, et al. *Phys. Rev. Lett.* 81:5068 (1998)
96. Morales A, et al. *Astropart. Phys.* 16:325 (2002)
97. Bernabei R, et al. *Phys. Lett. B* 515:6 (2001)
98. Ahmed Z, et al. *Phys. Rev. Lett.* 103:141802 (2009)
99. Armengaud E, et al. arXiv:1307.1488 [astro-ph.CO] (2013)
100. Cebrián S, et al. *Astropart. Phys.* 10:397 (1999)
101. Avignone FT III, Creswick RJ, Nussinov S. arXiv:1002.2718 [astro-ph.CO] (2010)
102. Ljubičić A, Kekez D, Krečak Z, Ljubičić T. *Phys. Lett. B* 599:143 (2004)

103. Derbin A, et al. *Phys. Rev. D* 83:023505 (2011)
104. Derbin A, Muratova V, Semenov D, Unzhakov E. *Phys. At. Nucl.* 74:596 (2011)
105. Derbin A, Drachnev I, Kayunov A, Muratova V. *JETP Lett.* 95:379 (2012)
106. Bellini G, et al. *Phys. Rev. D* 85:092003 (2012)
107. Moriyama S. *Phys. Rev. Lett.* 75:3222 (1995)
108. Krčmar M, et al. *Phys. Lett. B* 442:38 (1998)
109. Krčmar M, et al. *Phys. Rev. D* 64:115016 (2001)
110. Derbin A, et al. *Phys. Lett. B* 678:181 (2009)
111. Zioutas K, et al. *Phys. Rev. Lett.* 94:121301 (2005)
112. van Bibber K, McIntyre PM, Morris DE, Raffelt GG. *Phys. Rev. D* 39:2089 (1989)
113. Arik E, et al. *J. Cosmol. Astropart. Phys.* 0902:008 (2009)
114. Lazarus DM, et al. *Phys. Rev. Lett.* 69:2333 (1992)
115. Inoue Y, et al. *Phys. Lett. B* 536:18 (2002)
116. Moriyama S, et al. *Phys. Lett. B* 434:147 (1998)
117. Inoue Y, et al. *Phys. Lett. B* 668:93 (2008)
118. Zioutas K, et al. *Nucl. Instrum. Methods A* 425:480 (1999)
119. Kuster M, et al. *New J. Phys.* 9:169 (2007)
120. Abbon P, et al. *New J. Phys.* 9:170 (2007)
121. Aune S, et al. *J. Instrum.* 9:P01001 (2014)
122. Aune S, et al. *J. Instrum.* 8:C12042 (2013)
123. Arik E, et al. *Phys. Rev. Lett.* 107:261302 (2011)
124. Arik M, et al. *Phys. Rev. Lett.* 112:091302 (2014)
125. Andriamonje S, et al. *J. Cosmol. Astropart. Phys.* 0912:002 (2009)
126. Andriamonje S, et al. arXiv:0904.2103 [hep-ex] (2009)
127. Barth K, et al. *J. Cosmol. Astropart. Phys.* 1305:010 (2013)
128. Brax P, Lindner A, Zioutas K. *Phys. Rev. D* 85:043014 (2012)
129. Baum S, et al. arXiv:1409.3852 [astro-ph.IM] (2014)
130. Irastorza IG, et al. *J. Cosmol. Astropart. Phys.* 1106:013 (2011)
131. Armengaud E, et al. *J. Instrum.* 9:T05002 (2014)
132. Irastorza IG. *The International Axion Observatory LAXO. Letter of Intent to the CERN SPS Committee.* Tech. rep. CERN-SPSC-2013-022, SPSC-I-242. Geneva: CERN (2013)
133. Shilon I, Dudarev A, Silva H, Kate H. *IEEE Trans. Appl. Supercond.*, vol. 23 (2012)
134. Harrison FA, et al. *Astrophys. J.* 770:103 (2013)
135. Jakobsen AC, Pivovarov MJ, Christensen FE. *Proc. SPIE* 8861:886113 (2013)
136. Irastorza I, et al. *EAS Publ. Ser.* 53:147 (2012)
137. Dafni T, et al. *J. Phys. Conf. Ser.* 375:022003 (2012)
138. Dafni T, et al. *J. Phys. Conf. Ser.* 347:012030 (2012)
139. Isern J, Catalan S, Garcia-Berro E, Torres S. *J. Phys. Conf. Ser.* 172:012005 (2009)
140. Corsico AH, et al. arXiv:1205.6180 [astro-ph.SR] (2012)
141. Redondo J. Presented at Patras Workshop Axions, WIMPs, WISPs, CERN, Geneva. <http://axion-wimp2014.desy.de/> (2014)
142. Ehret K, et al. *Phys. Lett. B* 689:149 (2010)
143. Ehret K, et al. *Nucl. Instrum. Methods A* 612:83 (2009)
144. Purcell E. *Phys. Rev.* 69:681 (1946)
145. Haroche S, Kleppner D. *Phys. Today* 42:24 (1989)
146. Haroche S. *Phys. World* 4N3:33 (1991)
147. Hoogeveen F, Ziegenhagen T. *Nucl. Phys. B* 358:3 (1991)
148. Fukuda Y, Kohmoto T, Nakajima Si, Kunitomo M. *Prog. Cryst. Growth Charact. Mater.* 33:363 (1996)
149. Mueller G, Sikivie P, Tanner DB, van Bibber K. *Phys. Rev. D* 80:072004 (2009)
150. Jaeckel J, Ringwald A. *Phys. Lett. B* 659:509 (2008)
151. Caspers F, Jaeckel J, Ringwald A. *J. Instrum.* 4:P11013 (2009)
152. Betz M, et al. *Phys. Rev. D* 88:075014 (2013)
153. Ballou R, et al. arXiv:1410.2566 [hep-ex] (2014)

154. Battesti R, et al. *Phys. Rev. Lett.* 105:250405 (2010)
155. Inada T, et al. *Phys. Lett. B* 722:301 (2013)
156. Bähre R, et al. arXiv:1302.5647 [physics.ins-det] (2013)
157. Black E. *Am. J. Phys.* 69:79 (2001)
158. Lita AE, et al. *Proc. SPIE* 7681:76810D (2010)
159. Miller AJ, et al. *Opt. Express* 10:9102 (2011)
160. Dreyling-Eschweiler J. *A superconducting microcalorimeter for low-flux detection of near-infrared single photons*. PhD thesis, Dep. Phys., Univ. Hamburg. DESY-THESIS:2014-016. 230 pp. (2014)
161. Dreyling-Eschweiler J. In *Proceedings of the 10th Patras Workshop on Axions, WIMPs, and WISPs*, ed. E Tsesmelis, M Maroudas, p. 63. Hamburg, Ger.: DESY (2014)
162. Dreyling-Eschweiler J, et al. *J. Mod. Opt.* In press. doi:10.1080/09500340.2015.1021723 (2015)
163. Bottura L, de Rijk G, Rossi L, Todesco E. *IEEE Trans. Appl. Supercond.* 22:4002008 (2012)
164. Todesco E, Bottura L, de Rijk G, Rossi L. *IEEE Trans. Appl. Supercond.* 24:4004306 (2014)
165. Arias P, Jaeckel J, Redondo J, Ringwald A. *Phys. Rev. D* 82:115018 (2010)